Percorso dottorale sviluppato con il sostegno finanziario di NextGenerationEU:

Missione 4, Componente 2, Investimento 3.3, CUP B63C22000970009 Borsa MUR ex DM 352/2022, cofinanziata da Epigen Therapeutics srl

Dipartimento di Scienze Mediche Chirurgiche e Neuroscienze

Dottorato in Medicina Traslazionale e di Precisione

38° Ciclo

Coordinatore/Coordinatrice: Prof.ssa Anna Maria Di Giacomo

Molecular characterization of an anti-cancer demethylated cellular vaccine: coding and non-coding sequencing

Settore scientifico disciplinare: MED/06 – Medical Oncology

Candidato/a

Dott. Francesco Marzani

Università degli Studi di Siena

Firma digitale del/della candidato/a

Supervisore

Prof. Michele Maio

Department of Oncology University Hospital of Siena, Siena – Italy

Firmato digitalmente da
FRANCESCO MARZANI
28/03/2026 13:10:30
con la Firma Digitale cheFIRMA!

Co-supervisore

Dott.ssa Alessia Covre

Università degli Studi di Siena

Anno accademico di conseguimento del titolo di Dottore di ricerca

2024/25

Università degli Studi di Siena
Dottorato in Medicina Traslazionale e di Precisione
38° Ciclo

Data dell'esame finale
18/03/2026

Commissione giudicatrice
Marta Moretti – Ricercatrice, Sapienza Università di Roma
Massimo Guidoboni – Professore Ordinario, Università di Ferrara
Guido Sebastiani – Professore Associato, Università di Siena

Supplenti
Annamaria Di Giacomo – Professoressa Ordinaria, Università di Siena

TABLE OF CONTENTS

ABSTRACT

Therapeutic anticancer vaccines differ from preventive vaccines as they do not target factors associated with increased cancer risk; rather, they are designed to induce immunization against selected tumor antigens, thereby promoting recognition and elimination of malignant cells by the patient's immune system. In recent years, due to the strong biological rationale and encouraging preclinical results, numerous clinical studies have focused on the application of these strategies for cancer treatment. However, to date, only two therapeutic anticancer vaccines have received approval from regulatory authorities. Among the main factors limiting their efficacy are the restricted number of antigens that can be incorporated into a single vaccine formulation and their limited immunogenicity. Furthermore, the high costs and complexity of manufacturing processes hinder access to these treatments, thereby reducing the number of patients who may benefit from them.

To overcome these limitations, an innovative vaccine strategy (VAX) has been developed, based on the use of peripheral blood mononuclear cells (PBMCs) activated *in vitro* and subsequently treated with the epigenetic agent, decitabine, in order to modify their antigenic and immunological profile, enabling them to present antigens and induce an immune response. The present study aimed to characterize both the coding and non-coding transcriptome of multiple VAX preparations generated from healthy donor cells, in comparison with baseline PBMCs (T0) and with activated but untreated cells (untreated). To this end, total RNA extracted from each VAX, T0, and untreated preparation was analyzed using the Nanostring nCounter Sprint Profiler platform and RNA sequencing (Illumina NovaSeq 6000 System). The immunogenic potential of VAX was further evaluated at a functional level through ELISA assays for the detection of IgG antibodies specific for the tumor antigen New York esophageal squamous cell carcinoma (NY-ESO-1) in sera collected from BALB/c mice previously immunized with VAX.

The results indicate that VAX displays a gene expression profile characterized by the expression of multiple tumor-associated antigens (TAA), genes involved in antigen presentation pathways, costimulatory molecules, and pro-inflammatory cytokines induced during the preparation process. In addition, epigenetic remodeling of VAX led to the induction and/or upregulation of numerous transposable elements, which predominantly influence biological processes related to immune cell proliferation and activation, while also modulating pathways associated with cell adhesion, cytokine production, and response to interferon-γ (IFN-γ). These molecular findings are functionally supported by the presence of anti–NY-ESO-1 IgG antibodies in sera from VAX-immunized mice.

Overall, these data suggest that VAX possesses the capacity to elicit or enhance a specific immune response against a broad repertoire of tumor antigens, potentially resulting in therapeutic efficacy across multiple tumor histotypes and providing a solid rationale for future clinical translation.

1. INTRODUCTION

1.1 Therapeutic Cancer Vaccines

Cancer vaccines represent a promising frontier in oncological immunotherapy. Unlike prophylactic vaccines, which prevent virus-induced malignancies such as hepatitis B and human papillomavirus-related cancers, therapeutic cancer vaccines are designed to elicit a de novo immune response or amplify pre-existing antitumor immunity to eradicate established tumors and prevent recurrence (Ren et al., 2024; Lin et al., 2022). This is accomplished through the presentation of TAAs and the subsequent activation of antigen-specific cellular immune responses (Peng et al., 2025).

Therapeutic cancer vaccines aim to activate antigen-presenting cells (APCs), primarily dendritic cells (DCs), which process and present tumor antigens via major histocompatibility complex (MHC) molecules to naïve T cells. This presentation occurs in secondary lymphoid organs, leading to activation of cytotoxic $CD8^+$ T cells and helper $CD4^+$ T cells (Sheikhlary et al., 2024; Chekaoui et al., 2024). Activated T cells subsequently migrate into the tumor microenvironment (TME), where they mediate tumor cell killing through direct cytotoxicity and cytokine release (Fan et al., 2023).

In addition to T cells, B lymphocytes contribute to vaccine-induced antitumor immunity. Upon antigen recognition, naïve B cells differentiate into plasma cells that produce tumor-specific antibodies, potentially mediating tumor destruction through antibody-dependent cellular cytotoxicity (ADCC) and complement activation (Sheikhlary et al., 2024). Moreover, B cells may act as antigen-presenting cells, further amplifying adaptive immune responses (Hegoburu et al., 2025).

Despite extensive research and technological advances, the clinical efficacy of therapeutic cancer vaccines remains limited. Major barriers include insufficient immunogenicity, restricted antigenic breadth, tumor heterogeneity, immune tolerance, and tumor-induced immunosuppressive mechanisms. These limitations highlight the need for strategies capable of simultaneously expanding the antigenic repertoire and enhancing intrinsic immune activation.

1.2 Vaccine Platform-Based Classification

Therapeutic cancer vaccines can be classified according to the delivery platform employed.

Cell-based vaccines encompass whole tumor cell vaccines and dendritic cell (DC)-based approaches. Autologous tumor cell vaccines provide a broad repertoire of patient-specific antigens without prior antigen identification but require inactivation and immunostimulatory adjuvants to overcome their low intrinsic immunogenicity (Buonaguro and Tagliamonte, 2020; Bastin et al., 2023). Strategies such as genetic modification to secrete cytokines (e.g., GM-CSF in GVAX) have been explored to enhance immune activation.

DCs are considered the most potent antigen-presenting cells (APCs), playing a central role in initiating and regulating both innate and adaptive immune responses. Therefore, harnessing the diversity and antigen-

presenting capacity of DCs holds significant promise for enhancing the efficacy of cancer vaccines (Lee et al., 2023). Sipuleucel-T (Provenge®), approved for metastatic castration-resistant prostate cancer, involves ex vivo loading of autologous APCs with a recombinant fusion antigen before reinfusion. More recent approaches include DCs pulsed with tumor lysate, peptides, or mRNA, aiming to broaden antigen presentation and improve immunogenicity.

Peptide-based vaccines consist of synthetic tumor-derived epitopes. Short peptides (8-11 amino acid epitopes) primarily induce $CD8^+$ T cell responses, whereas long peptides (20-35 amino acids) require processing by APCs and promote coordinated $CD4^+$ and $CD8^+$ activation, resulting in more durable immunity (Shah et al., 2025).

Nucleic acid-based vaccines, including DNA and mRNA platforms, enable *in vivo* antigen expression and presentation through both MHC class I and II pathways. The rapid development of mRNA vaccine technologies has accelerated their application in oncology, particularly in personalized neoantigen-based approaches (Ren et al., 2024). Among nucleic acid vaccines, the prominent Moderna's and Merck's mRNA-4157, demonstrate to prolong recurrence-free survival in combination with pembrolizumab versus pembrolizumab monotherapy in patients with resected high-risk melanoma further showing a manageable safety profile (Weber et al., 2024).

Viral vector-based vaccines utilize engineered viruses to deliver tumor antigens and stimulate strong innate and adaptive immune responses. Oncolytic viruses further combine direct tumor lysis with immune activation, as exemplified by Talimogene laherparepvec (T-VEC) (Liu et al., 2022; Strum et al., 2024).

Despite these advances, clinical efficacy remains limited in many settings, underscoring the need for strategies that simultaneously expand antigenic diversity and enhance intrinsic immunogenicity.

1.3 Antigen-based Classification of Vaccines

Antigen selection represents a critical step in cancer vaccine design. Ideally, vaccine antigens should be highly immunogenic, selectively expressed in tumor cells, and essential for tumor survival to limit immune escape. Antigen immunogenicity depends on their expression level, efficiency of proteasomal processing, peptide–MHC binding affinity, and T cell receptor recognition (Mauriello et al., 2025). Moreover, antigens should be explicitly expressed in all cancer cells and not in normal cells and necessary for the survival of cancer cells thus limiting immune escape via antigen downregulation (Hollingsworth and Jansen, 2019).

Two types classes of antigens can be used to generate a cancer vaccine: TAAs and tumor-specific antigens (TSA).

TAAs are overexpressed or aberrantly expressed in malignant cells but may also be present at low levels in normal tissues (Zhao et al., 2021). These include differentiation antigens (e.g., PSA, tyrosinase), overexpressed antigens (e.g., HER2, hTERT, MUC-1), and cancer-testis antigens (CTA) (e.g., melanoma-associated antigen

(MAGE), New York esophageal squamous cell carcinoma-1 (NY-ESO-1), and synovial sarcoma X chromosome breakpoint (SSX) family members) (Ruzzi et al., 2025; Ai et al., 2023; Naik et al., 2024).

TSA encompass a diverse group of antigens that arise from tumor-restricted molecular alterations and are absent from normal tissues (Zhao et al., 2021).

Although multiple molecular mechanisms may generate TSA, including somatic mutations, structural rearrangements, and aberrant RNA processing (Xie et al., 2023; Guan et al., 2023), not all tumors harbor sufficient mutational burden to produce highly immunogenic neoantigens. This limitation is particularly relevant in tumors characterized by low mutation rates, underscoring the need for alternative sources of tumor-restricted antigenicity.

1.4 Cancer-Testis Antigens (CTA)

Among TAAs, CTA represent one of the most attractive targets for cancer immunotherapy. CTA are typically expressed in immune-privileged tissues such as testis and placenta but are aberrantly expressed in a wide range of malignancies. Their restricted expression pattern in normal tissues, combined with their high immunogenicity, makes them particularly suitable targets for therapeutic vaccination. Among more than 200 CTA genes identified in the human genome, MAGE family members and NY-ESO-1 have been extensively studied. These antigens are capable of eliciting both humoral and cellular immune responses. They contain epitopes presented by multiple HLA class I and II molecules, enabling activation of $CD8^+$ cytotoxic T lymphocytes and $CD4^+$ helper T cells, which are essential for the priming, amplification, and maintenance of antitumor immunity (Zhao et al., 2021; Wermke et al., 2025). In addition, the simultaneous humoral and cytotoxic responses against MAGE-A3 (Slingluff et al., 2016; Pujol et al., 2015) and NY-ESO-1 (Raza et al., 2020) frequently observed in cancer patients, further revealed the natural ability of CTA to trigger a specific antitumor immune response, either spontaneously or following vaccination.

CTA expression is tightly regulated by epigenetic mechanisms, especially DNA methylation (Zhao et al., 2021). In healthy somatic tissues, promoter hypermethylation maintains CTA genes in a transcriptionally silent state. During tumorigenesis, global DNA hypomethylation leads to their derepression. Importantly, hypomethylating agents such as decitabine have been shown to pharmacologically induce CTA expression (Fazio et al., 2018).

The inducibility of CTA through epigenetic modulation provides a rationale for exploiting hypomethylating agents to expand the antigenic repertoire of vaccine platforms.

1.5 Transposable Elements (TE) and Endogenous Viral Elements as Sources of Tumor Antigenicity

A recently recognized and highly promising source of tumor-specific antigenicity involves the reactivation of TE and endogenous viral elements (EVE) (Lanciano and Cristofari, 2024; Garde et al., 2025). TEs are repeated sequences that can disperse and replicate through a cut-and-paste or copy-and-paste mechanism and constitute nearly half of the human genome. They include retrotransposons and DNA transposons. Retrotransposons are subdivided into long terminal repeat (LTR) and non-LTR elements; the latter include long interspersed nuclear elements (LINE) and short interspersed nuclear elements (SINE), while LTR elements encompass endogenous retroviruses (ERV) (Schmidleithner et al., 2025).

TE can significantly contribute to genomic instability, therefore, in normal somatic tissues, TE activity is tightly repressed by epigenetic mechanisms, particularly DNA methylation (Schmidleithner et al., 2025). However, during oncogenesis, global epigenetic dysregulation frequently leads to TE derepression (Shah et al., 2023).

TE reactivation may contribute to tumor immunogenicity through multiple mechanisms. Transcriptionally active TEs can generate chimeric TE-gene transcripts, novel open reading frames, alternative translation start sites, and peptide extensions (Shah et al., 2023). These products may be processed and presented by MHC molecules, functioning as TSA (Lanciano and Cristofari, 2024). High-throughput analyses have identified thousands of TE-derived transcripts across different tumor types, with LINE-1 and LTR elements being particularly prevalent (Shah et al., 2023; Liang et al., 2024).

In addition to serving as antigenic sources, TE reactivation can induce “viral mimicry” state. Accumulation of double-stranded RNA derived from endogenous retroelements may activate innate immune sensing pathways, including cytosolic nucleic acid sensors such as cGAS-STING, leading to type I interferon signaling and interferon-stimulated gene expression. This process enhances antigen presentation machinery, promotes inflammatory cytokine production, and may increase tumor immunogenicity (Nesci et al., 2025).

Importantly, T cell responses directed against EVE-derived peptides have been detected in cancer patients but not in healthy individuals, underscoring their tumor-restricted immunogenic potential. These findings support the exploration of TE-derived antigens as targets for cancer vaccine development, particularly in tumors with low mutational burden.

1.6 Limitations and Resistance Mechanisms of Cancer Vaccines

Despite significant technological advances across multiple vaccine platforms, the clinical efficacy of therapeutic cancer vaccines has remained limited. Several resistance mechanisms inherent to tumor biology contribute to this modest success.

A major barrier is the heterogeneity of the tumor microenvironment (TME). The TME is composed of diverse cellular populations, including immunosuppressive subsets such as regulatory T cells (Tregs), myeloid-derived suppressor cells (MDSCs), and tumor-associated macrophages (TAMs) (Kaczmarek et al., 2023). The complex interplay among these cells can suppress antigen presentation and inhibit cytotoxic T cell activity, thereby facilitating immune evasion and reducing vaccine effectiveness.

In addition, tumor cells frequently exploit immune checkpoint pathways to dampen T cell responses. Overexpression of inhibitory molecules such as PD-1/PD-L1 and CTLA-4 limits T cell activation and promotes immune escape (Fan et al., 2023). The use of monoclonal antibodies targeting these checkpoints has demonstrated clinical benefit and is increasingly being evaluated in combination with cancer vaccines to enhance antitumor immunity (Kamath, 2021). Several clinical trials combining personalized neoantigen vaccines with PD-1 blockade in melanoma and non-small cell lung cancer (NSCLC) have reported improved immune responses and progression-free survival. For example, the mRNA-based vaccine BNT111 targeting NY-ESO-1, MAGE-A3, tyrosinase, and TPTE has shown encouraging immunogenicity in advanced melanoma when administered alongside immune checkpoint inhibitors. Similarly, the mRNA-4157 vaccine is under evaluation in combination with pembrolizumab in melanoma and other solid tumors (Ren et al., 2024).

Beyond immune suppression, tumor heterogeneity represents a major obstacle to effective vaccination. Distinct tumor subclones may express different antigenic profiles, enabling immune escape of antigen-negative variants (Fan et al., 2023). Immunization strategies targeting a broad set of antigens have been proposed to address this issue, increasing the likelihood that multiple tumor clones are simultaneously recognized. However, vaccine-induced immune pressure may also promote immunoediting, selecting for tumor subclones with reduced antigen expression and lower immunogenicity.

Whole-cell vaccines inherently provide broad antigen exposure by presenting the entire repertoire of TAAs (Kaczmarek et al., 2023). While this approach may be advantageous in heterogeneous tumors, it presents important limitations, including the requirement for sufficient tumor material, logistical challenges in collection and manufacturing, and stringent regulatory constraints under Good Manufacturing Practice (GMP) standards. Moreover, the presence of abundant non-tumor self-antigens may dilute tumor-specific epitopes and potentially promote immune tolerance (Buonaguro and Tagliamonte, 2020).

Multi-epitope peptide formulations and personalized neoantigen vaccines have been developed to expand antigenic coverage while maintaining specificity. Although promising, these approaches are associated with formulation complexity, HLA restriction constraints, dependence on potent adjuvants, and, in the case of personalized vaccines, time-consuming sequencing, bioinformatic prediction, and individualized manufacturing (Fan et al., 2023).

Additional challenges include the frequent enrollment of patients with advanced-stage disease, in whom profound immune suppression may compromise vaccine responsiveness (Kamath, 2021). Age-related immune

senescence further reduces T cell functionality and increases the prevalence of immunosuppressive cell populations, potentially diminishing vaccine efficacy (Kaczmarek et al., 2023).

Collectively, these limitations underscore two central challenges in cancer vaccine development: achieving sufficiently broad antigenic coverage to overcome tumor heterogeneity, and enhancing intrinsic immunogenicity within an immunosuppressive microenvironment, while maintaining feasible and scalable manufacturing processes.

One emerging strategy to address these challenges involves epigenetic reprogramming to expand the endogenous antigenic repertoire and simultaneously enhance immune activation.

1.7 Epigenetic Remodeling as a Strategy to Enhance Vaccine Immunogenicity

Epigenetic modifications are heritable yet reversible chemical alterations that regulate chromatin structure and gene transcription without modifying the underlying DNA sequence (Dai et al., 2024). These mechanisms, including DNA methylation, histone modifications, chromatin remodeling, and non-coding RNA regulation, coordinate gene expression programs essential for cellular identity and differentiation. Their dysregulation represents a hallmark of cancer (Gibney and Nolan, 2010).

Among these mechanisms, DNA methylation is one of the most extensively characterized. It consists of the covalent addition of a methyl group at the C5 position of cytosine residues, predominantly at CpG dinucleotides, generating 5-methylcytosine (5mC) (Moore et al., 2013). In mammalian genomes, most CpG sites are methylated, and this modification is generally associated with transcriptional repression (Angeloni and Bogdanovic, 2021). DNA methylation can directly interfere with transcription factor binding or recruit methyl-CpG-binding proteins that promote chromatin compaction and stable gene silencing.

In physiological conditions, DNA methylation plays a central role in development, genomic imprinting, X-chromosome inactivation, and suppression of TE. In cancer, however, epigenetic landscapes become profoundly altered, often characterized by global hypomethylation alongside focal promoter hypermethylation. This imbalance contributes both to oncogene activation and silencing of tumor suppressor and immune-related genes.

DNA methylation patterns are established and maintained by DNA methyltransferases (DNMTs). DNMT1 primarily ensures maintenance methylation during DNA replication, while DNMT3A and DNMT3B mediate de novo methylation (Moore et al., 2013; Yang et al., 2023). Pharmacologic inhibition of DNMTs has emerged as a strategy to reverse aberrant methylation and reprogram transcriptional states.

1.8 DNMT Inhibitors and Immunomodulation

DNA methyltransferase inhibitors (DNMTi) are divided into nucleoside analogs, such as decitabine (5-aza-2'-deoxycytidine) and azacitidine, and non-nucleoside inhibitors. Decitabine, a cytidine analog incorporated into DNA during replication, irreversibly traps DNMT1, leading to its degradation and progressive passive demethylation across subsequent cell divisions.

Beyond its cytotoxic effects at high doses, low-dose decitabine exerts profound immunomodulatory activity. By inducing hypomethylation, it can reactivate silenced genomic regions, including:

- CTA, such as MAGE and NY-ESO-1 (Dai et al., 2024; Fazio et al., 2018);
- endogenous retroviruses (ERVs) and other TE (Patel et al., 2025; Kong et al., 2019);
- genes involved in antigen processing and presentation (Fazio et al., 2018);
- interferon-stimulated genes and pro-inflammatory chemokines (Fazio et al., 2018).

Reactivation of endogenous retroelements can generate double-stranded RNA species, triggering innate immune sensing pathways and type I interferon responses through mechanisms often described as “viral mimicry.” This state enhances antigen presentation and promotes a pro-inflammatory microenvironment favorable for immune recognition (Dhillon et al., 2023).

Importantly, RNA sequencing studies have demonstrated that decitabine treatment upregulates multiple classes of TE, including LINEs, SINEs, and LTR/ERV elements. In some contexts, TE-derived transcripts generate peptides presented by MHC molecules, further expanding the antigenic landscape (Patel et al., 2025; Kong et al., 2019).

Thus, DNMT inhibition does not merely reverse epigenetic silencing but can reshape the immunogenic profile of cells by simultaneously expanding antigen diversity and activating innate immune signaling pathways.

1.9 MicroRNAs and Epigenetic–Immune Crosstalk

MicroRNAs (miRNAs) are small non-coding RNAs (~22 nucleotides) that regulate gene expression post-transcriptionally influencing numerous physiological and pathological processes (Shang et al., 2023). Through partial sequence complementarity, miRNAs induce translational repression or mRNA degradation.

miRNA expression is tightly regulated at transcriptional and post-transcriptional levels and is itself influenced by DNA methylation (Glaich et al., 2019). Hypermethylation of miRNA gene promoters can suppress their expression, whereas hypomethylation may induce their upregulation. Conversely, miRNAs can regulate the expression of epigenetic modifiers, including DNMTs, establishing bidirectional feedback loops between epigenetic and post-transcriptional regulatory layers.

In the context of cancer immunology, miRNAs modulate multiple processes relevant to vaccine efficacy, including antigen presentation, T cell activation, cytokine signaling, and immune checkpoint regulation. Therefore, epigenetic interventions that alter DNA methylation patterns may also reshape miRNA networks, contributing to coordinated remodeling of immune-related gene expression (Fuso et al., 2020; Glaich et al., 2019).

2. AIM OF THE THESIS

Cancer is among the leading causes of death worldwide, with almost 20 million new cases reported in 2022 and an estimated increase to 33 million by 2050. Despite the availability of multiple therapeutic options, cancer remains a major cause of mortality, and a substantial proportion of patients still do not benefit from current treatments. Therefore, the development of innovative therapeutic strategies and novel drug combinations is essential. In this context, therapeutic cancer vaccines currently represent a promising approach. Indeed, such vaccines can elicit a specific immune response and enhance pre-existing immunity against a broad spectrum of tumor antigens, enabling the recognition and the killing of cancer cells. However, limitations related to antigen selection, reduced immunogenicity, and the time and cost required for production decrease vaccine efficacy and restrict the number of patients who can benefit from this treatment.

The present study aimed to comprehensively characterize the molecular properties of an innovative therapeutic cancer vaccine (VAX), based on activated human peripheral blood mononuclear cells (PBMCs) epigenetically reprogrammed with the DNA hypomethylating agent decitabine. Specifically, the first objective was to define the coding and non-coding (e.g., miRNA) transcriptomic landscape of different VAX preparations generated from healthy donors, and to compare them with baseline PBMCs (T0) and activated but untreated cells (untreated). Through transcriptomic profiling using NanoString technology and RNA sequencing, we investigate whether the preparation process induces the expression of TAA, antigen presentation machinery, co-stimulatory molecules, pro-inflammatory cytokines, and other immune-related pathways. A second objective was to investigate the impact of epigenetic remodeling on transposable elements (TE) expression and to assess how TE upregulation may influence immune-related biological processes, including leukocyte proliferation, T-cell activation, cytokine production, interferon-γ response, and cell adhesion pathways. Finally, the study aimed to functionally evaluate the immunogenic potential of VAX *in vivo* by assessing the induction of humoral responses against the human TAA NY-ESO-1, measured as antigen-specific IgG production in immunized BALB/c mice. Overall, this study was designed to determine whether VAX can generate a broad immunogenic antigen profile along with adjuvant/costimulatory stimuli capable of eliciting or enhancing tumor-specific immune responses, thereby providing a strong rationale for its further translational development.

3. MATERIAL AND METHODS

3.1 Preparation of Vaccine (VAX) and control cells

PBMCs were purchased from Tebu-Bio (Tebu-Bio Srl, Milan, Italy). Human cells were thawed according to the manufacturer's instructions, counted, and seeded at a density of 2×10^6 cells/mL in 75 cm^2 tissue culture flasks (EuroClone S.p.A., Milan, Italy). Cells were maintained in Iscove's Modified Dulbecco's Medium (EuroClone S.p.A., Milan, Italy) supplemented with 10% heat-inactivated human AB serum (HIV-tested; EuroClone S.p.A., Milan, Italy), 2mM L-glutamine (Euroclone, Milan, Italy), 100 U/mL penicillin and 100 µg/mL streptomycin (Euroclone, Milan, Italy), recombinant human interleukin-2 (IL-2; 100 U/mL; Proleukin®, Novartis, Basel, Switzerland), and anti-CD3 monoclonal antibody (OKT3; 50 ng/mL; Miltenyi Biotec, Bergisch Gladbach, Germany). VAX preparation consisted of treatment with 1µM of 5-aza-2′-deoxycytidine (5-AZA-CdR; Sigma-Aldrich, St. Louis, USA; #A3656-5MG) 24 hours after plating. The treatment with 5-AZA-CdR was repeated every 12 hours for the following two days for a total of 4 rounds of pulses. On Day 6, both untreated and treated cells were collected. Two control conditions were included:

- T0 sample, representing the basal condition, consisting of PBMCs immediately frozen in TRIzol™ reagent (Invitrogen, CA, USA) upon isolation.
- Untreated sample, subjected to the same *ex vivo* activation protocol as VAX but without exposure to 5-aza-2′-deoxycytidine.

3.2 Isolation of total RNA

Total RNA was isolated from $2x10^6$ cells *per* sample using 1 mL of TRIzol reagent (Invitrogen, CA, USA). The samples were incubated for 10 minutes at room temperature (RT), allowed TRIzol to degrade nucleoprotein complexes while preserving intact nucleic acids. Subsequently, 200 µL of chloroform ($CHCl_3$) (Carlo Erba Reagenti, Milan, Italy) were added and for 15 seconds tubes were forcibly shaken, incubated for 3 minutes at RT and then centrifugated at 491 x *g* for 15 minutes at 4°C. The previous steps allow the solution to separate in three distinct phases: aqueous, intermediate and organic. The aqueous phase was carefully collected and transferred to new tubes, where 600 µL of isopropyl alcohol (Carlo Erba Reagenti, Milan, Italy) were added to precipitate RNA. The samples were gently inverted 5 times, incubated at RT for 10 minutes and centrifugated again at 491 x *g* for 10 minutes at 4°C. After centrifugation, the supernatants were carefully aspirated, and RNA pellets were washed with 1 mL of 75% ethanol for ensuing centrifugation at 491 x *g* for 5 minutes at 4°C. Finally, the supernatants were discarded, and the pellets were left to dry for 5-20 minutes, before being resuspended in an appropriate volume (10–50 µL) of RNase-free water (Invitrogen, CA, USA), depending on their size. RNA concentration was quantified, and purity were assessed with NanoDrop™ One (Thermo Fischer Scientific, DE, USA). High-quality RNA extraction was confirmed by A260/A280 (nucleic acid/protein) ratios ≥ 2 and A260/A230 (nucleic acid/reagents) ratios ≥ 1.8.

3.3 RNA digestion with DNAse I

To obtain an RNA sample free of DNA contamination, digestion with 10 U/µL DNAseI is performed. 2 µg of total RNA from each sample was digested, in a final volume of 20 µL H2O. A 4 µL-mix consisting of 2 µL of digestion buffer (Tris-HCl 200 mM pH 8, KCl 500 mM, MgCl2 20 mM) and 2 µL of DNAse I recombinant enzyme 10 U/µL (Roche, Basel, Switzerland) were added to each sample and incubated for 30 minutes at RT. Then, to inactivate DNAse I, 2 µL of EDTA 25mM were added to samples and a further 10 minute-incubation at 65°C was performed.

3.4 Reverse transcription of RNA with hexamer primers

Previously digested RNA samples were reverse transcribed using a two-step reaction procedure to obtain complementary DNA (cDNA). A total of 6 µL of digested RNA, corresponding to 0.545 µg, was added to 5µL of a first reaction mix containing 1µL of Random Primers 0.5 µg/µL, (Promega, WI, USA) and 4µL of dNTPs 10 mM (dATP, dGTP, dCTP, and dTTP; Invitrogen, CA, USA), and incubated for 5 minutes at 65°C. 9 µL of second reaction mix, consisting of 4 µL of Strand Buffer 5X (Tris-HCl 250 mM pH 8.3, KCl 375 mM, MgCl2 15 mM; Invitrogen, CA, USA), 2 µL of DTT 0.1mM (Dithiothreitol; Invitrogen, CA, USA), 2 µL of RNAse inhibitor enzyme 40 U/µL (Invitrogen, CA, USA), and 1 µL of Murine Leukemia Virus Reverse Transcriptase enzyme 10000 U/mL (M-MLV RT; Invitrogen, CA, USA), were added. The tubes were then subjected to 3 incubation steps: 25°C for 10 minutes, 37°C for 50 minutes, and 70°C for 15 minutes. Finally, 80 µL of RNase-free water were added to achieve a final cDNA concentration of 5.45 ng/µL in a total volume of 100 µL.

3.5 nCounter® gene expression analysis

Total RNA extracted from VAX, untreated and T0 preparations was analyzed using the nCounter® SPRINT Profiler (NanoString Technologies, Seattle, USA). The PanCancer Immune Profiling Panel gene expression panel was used to simultaneously evaluate the expression of 770 mRNA targets, starting from the recommended RNA input quantity of 100 ng. These targets include transcripts representative of major immune cell populations, enabling high-throughput profiling of the tumor immune microenvironment and the identification of clinically actionable gene expression signatures in cancer immunotherapy. Overnight hybridization was set up at 65°C, using the Applied Biosystems™ Veriti 96-Well Thermal Cycler (Thermo Fischer Scientific, DE, USA). Raw data were processed into a signature matrix using nSolver Analysis Software version 4.0 (NanoString Technologies, Seattle, USA). Background noise was removed by subtracting negative control counts from the raw data. Data were then normalized to housekeeping genes with a coefficient of variation (%CV) lower than 30%. Lastly, advanced analysis was carried out to estimate the differential expression of RNA targets between VAX, untreated, and T0 samples.

3.6 nCounter® miRNA expression analysis

MiRNAs expression profile was analyzed from 100 ng of total RNA by the nCounter SPRINT Profiler, using the NanoString miRNA gene expression panel, which detects up to 798 microRNA targets (NanoString Technologies, Seattle, USA). Raw data (average counts) were analyzed by the nSolver software. Background noise was removed by subtracting the negative control with the highest count to raw data. Data were then normalized using the CodeSet Content Normalization Top 100 method, which scales counts to the geometric mean of the 100 most highly expressed miRNAs across all samples, excluding miRNAs with a % CV below 30% from the normalization calculation.

3.7 Analysis of differentially expressed genes and miRNAs

Counts of target genes or miRNAs were exported from the nSolver™ software associated with the nCounter® SPRINT Profiler system and subjected to preprocessing. This step included Log_2 transformation of the data. Log_2 transformation converts raw expression values to their base-2 logarithmic equivalents, facilitating the analysis of data spanning multiple orders of magnitude and improving interpretability in the transcriptomic studies. Quantile normalization was then applied to ensure that observed differences in gene expression across samples were primarily attributable to biological variation rather than technical bias, thereby enhancing the robustness and reliability of downstream analyses. Data were then filtered based on variability, excluding genes and miRNAs with an interquartile range (IQR) below the mean IQR. Differential expression analysis was performed using a Student's t-test, followed by multiple testing correction according to the Benjamini–Hochberg false discovery rate (FDR) method. Furthermore, genes targeted by the set of differentially expressed miRNAs were identified through miEAA 2.0 software (Aparicio-Puerta et al., 2023).

3.8 Ingenuity pathway analysis (IPA)

Ingenuity pathway analysis (IPA) (QIAGEN, Hilden, Germany) (Krämer et al., 2014), was performed to identify canonical pathways (CPs) activated (Z-score ≥ 2) or inhibited (Z-score ≤ -2), based on differentially expressed genes (DEGs) between VAX, T0 and untreated samples. Gene Ontology (GO) term enrichment analysis for biological process (BPs) was performed on the DEGs by the Enrichr web tool (Chen et al., 2013; Kuleshov et al., 2016; Xie et al., 2021). Statistically significant BPs (p-value <0.05) were ranked by their combined score, and the top 100 terms were selected for further analysis. Data visualization was performed using GraphPad Prism 8.0 (GraphPad Software Inc., San Diego, CA, USA) for box-and- whisker-plots, and using the ggplot2 R package for dot plots.

3.9 NY-ESO-1 expression analysis through quantitative RT-PCR

Quantitative real time-PCR was performed on 20 ng cDNA in a final volume of 20 µL containing SYBR Green Master Mix (Applied Biosystem, CA, USA) and specific primers for the detection of the target gene NY-ESO-

1 and the reference gene β-actin, at 95°C for 10 min, followed by 45 cycles at 95°C for 15 s and at 60°C for 1 min, followed by dissociation performed at 95°C for 15 s, 60°C for 1 min and 95°C for 15 s. Absolute quantifications were carried out using calibration curves, based on known scalar dose concentrations of recombinant plasmid DNA containing the corresponding gene to amplify. The copy number of specific gene was determined extrapolating values from the calibration curves, and then number of NY-ESO-1 copies were normalized to the number of β-actin copies. Gene expression was considered: positive if numbers of NY-ESO-1/β-actin molecules were ≥1E-04; upregulated or down-regulated if its positive expression was increased or decreased at least twice (Fold Change (FC) ≥ 2 or FC ≤ 0.5), respectively. QuantStudio™ 5 Real-Time PCR System (Applied Biosystems™, CA, USA) and its analysis software were used to conduct the quantitative RT-PCR analyses.

Sequences of utilized primers are listed in table 1.

Table 1. β-Actin and NY-ESO-1 primers sequences for quantitative RT-PCR

Gene name	Forward sequence	Reverse sequence
β-ACTIN	5'-CGAGCGCGGCTACAGCTT-3'	5'-CCTTAATGTCACGCACGATT-3'
NY-ESO-1	5'-TGCTTGAGTTCTACCTCGCCA-3'	5'-TATGTTGCCGGACACAGTGAA-3'

3.10 Ex vivo enzyme-linked immunosorbent assay

The enzyme-linked immunosorbent assay (ELISA) was performed on mouse sera collected before vaccination and after the first, second, third, and fourth immunizations with VAX. 96-well plates were coated overnight at +4°C with 1 µg/mL Recombinant Human Cancer/testis antigen 1 peptide (RayBiotech, GA, USA; #230-00634) in 50 µL/well 1X PBS. Plates were blocked for 2 hours at 37°C with 100 µL 1X PBS (Thermo Fischer Scientific, DE, USA) +1% BSA (Sigma-Aldrich, MO, USA) to prevent nonspecific binding and washed three times with 1X PBS + 0.05% Tween 20 (Bio-Rad, CA, USA). Serum samples were diluted 1:50 in 1X PBS+ 0.05% Tween20, followed by 1:2 serial dilutions directly in the plates. Mouse anti-human CTAG1B (NY-ESO-1) IgG (Origene, MD, USA) at 1:10,000 served as positive control, and sera collected prior to treatment (n=12) as negative control. Plates were incubated 2 hours at 37°C, washed, and incubated with goat anti-mouse IgG (H+L) HRP-conjugated detection antibody (Bio-Rad) at 1:10,000 for 1 hour at 37°C. After washing, substrate solution (Milli-Q water, pH ≈ 4.0) containing 0.25 mg/mL ABTS, 0.03% hydrogen peroxide, 17 mM sodium citrate, and 33 mM citric acid was added (100 µL/well). The reaction was stopped with 100 µL/well of 100 mM citric acid in Milli-Q water, and absorbance was read at 415 nm using the iMark™ Microplate Reader (Bio-Rad, CA, USA).

3.11 RNA-Sequencing and data analysis

Five additional VAX preparations and the corresponding control conditions (T0 and untreated) were generated as described in Section 3.1. A total of 500 ng of total RNA from each sample was shipped to Genomix4life S.R.L. (Baronissi, Salerno, Italy) for Next generation sequencing. RNA concentration was determined by using NanoDropOne spectrophotometer (Thermo Fisher), Qubit (Thermo Fisher) and its quality assessed with the TapeStation 4200 (Agilent Technologies). Indexed libraries were prepared from 200 ng purified RNA with Illumina Stranded Total RNA Prep with Ribo-Zero Plus (Illumina) according to the manufacturer's instructions. Libraries were quantified using the TapeStation 4200 (Agilent Technologies) and and Qubit fluorometer (Invitrogen Co.), then pooled such that each index-tagged sample was present in equimolar amounts. The pooled samples were subject to cluster generation and sequencing using an Illumina NovaSeq6000 System (Illumina) in a 2x101 paired-end format.

Raw FASTQ files were subjected to quality control using FastQC (v0.11.8), and low-quality reads were removed. High-quality reads were aligned to the human reference genome (GRCh38/hg38) using STAR (v2.7.0b) (Dobin et al., 2013), and gene-level expression quantification was obtained after the alignment step.

Downstream analyses were conducted in the R statistical environment. Count data were normalized, and differential gene expression across experimental conditions was assessed using DESeq2 (Love et al., 2014). Genes with adjusted p-value < 0.01 (Benjamini–Hochberg correction) and log2 fold change > 2 were considered differentially expressed.

Expression of genomic repetitive DNA features was quantified using the featureCounts function from the Rsubread package (Liao et al., 2019), enabling both useMetaFeatures and countMultiMappingReads options. A custom GTF annotation file describing repetitive elements was used for this purpose. Genomic coordinates for repetitive DNA features, including long interspersed nuclear elements (LINEs), short interspersed nuclear elements (SINEs), and long terminal repeat (LTR) elements, were obtained from the UCSC RepeatMasker annotation (GRCh38/hg38) via the AnnotationHub R package (Morgan and Shepherd, 2025). Repetitive elements overlapping annotated exonic regions were excluded from the analysis. For each repetitive element class, multi-mapping reads were weighted by the number of genomic mapping sites, averaged across features, and subsequently log2-transformed prior to downstream analyses. Differential expression of repetitive DNA features was assessed using the Mann–Whitney–Wilcoxon test. Repetitive DNA loci were considered differentially expressed if they exhibited an adjusted p-value < 0.01 (Benjamini–Hochberg correction) and an absolute log2 fold change greater than 2.

4. RESULTS

4.1 Gene expression characterization of VAX preparations

To characterize epigenetic remodeling–induced changes in the gene expression profile of VAX following *ex vivo* activation of PBMCs, NanoString nCounter analysis was performed using the PanCancer Immune Profiling Panel on total RNA extracted from #9 VAX preparations vs. the T0 and the untreated conditions. Differentially expressed genes (DEGs) analyses were conducted separately for VAX vs. T0 and VAX vs. untreated.

Comparative analysis of VAX vs. T0 identified 163 upregulated and 163 down-regulated genes, as shown in Figure 1.

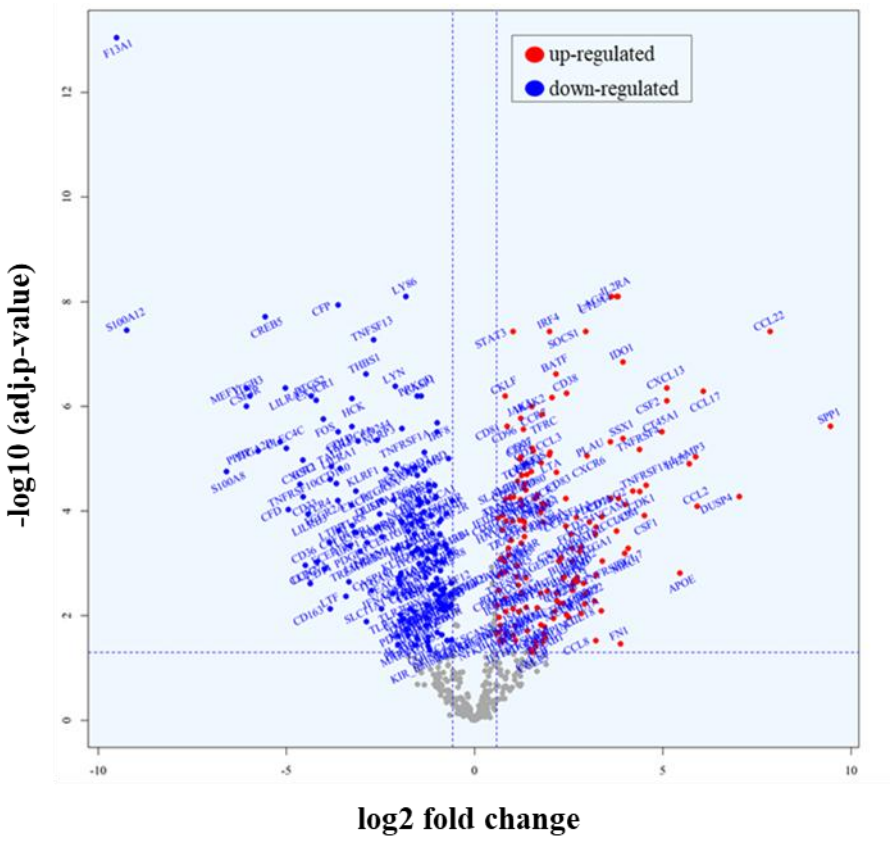

Figure 1. Volcano plot illustrating DEGs between VAX and the original PBMC (T0).

Each point corresponds to a gene, plotted according to its log2 fold change (x-axis) and statistical significance, expressed as the –log10 of the adjusted p-value (y-axis). Differential expression analysis was performed using a two-sample t-test, followed by correction for multiple comparisons via the Benjamini-Hochberg false discovery rate (FDR) procedure. Genes with log2 fold change ≥ 0.58 (FC = 1.5) and an adjusted p-value corresponding to –log10(FDR) ≥ 1.3 (FDR ≤ 0.05) *were considered upregulated. Whereas genes with a log2 fold change ≤ -0.58 (FC = -1.5) and an adjusted p-value corresponding* to –log10(FDR) ≥ 1.3 (FDR ≤ 0.05) *were considered down-regulated. Significantly upregulated genes are shown in red, while downregulated genes are depicted in blue.*

The ten most significantly upregulated genes were LAG3, IL2RA, CTLA4, CCL22, STAT3, IRF4, SOCS1, IDO1, BATF, and CXCL13, with adjusted p-values ranging from 7.93×10^{-09} to 4.48×10^{-07}. The ten most significantly downregulated genes were F13A1, LY86, CFP, CREB5, S100A12, TNFSF13, THBS1, LYN, MEFV, and LILRA5, with adjusted p-values ranging from 8.98×10^{-14} to 4.48×10^{-07}. Based on the high number of DEGs (n = 326) identified in VAX vs. T0 conditions, Ingenuity Pathway Analysis (IPA) software was used to predict activated (Z-score ≥ 2) and inhibited (Z-score ≤ −2) canonical pathways (CPs) (Figure 2).

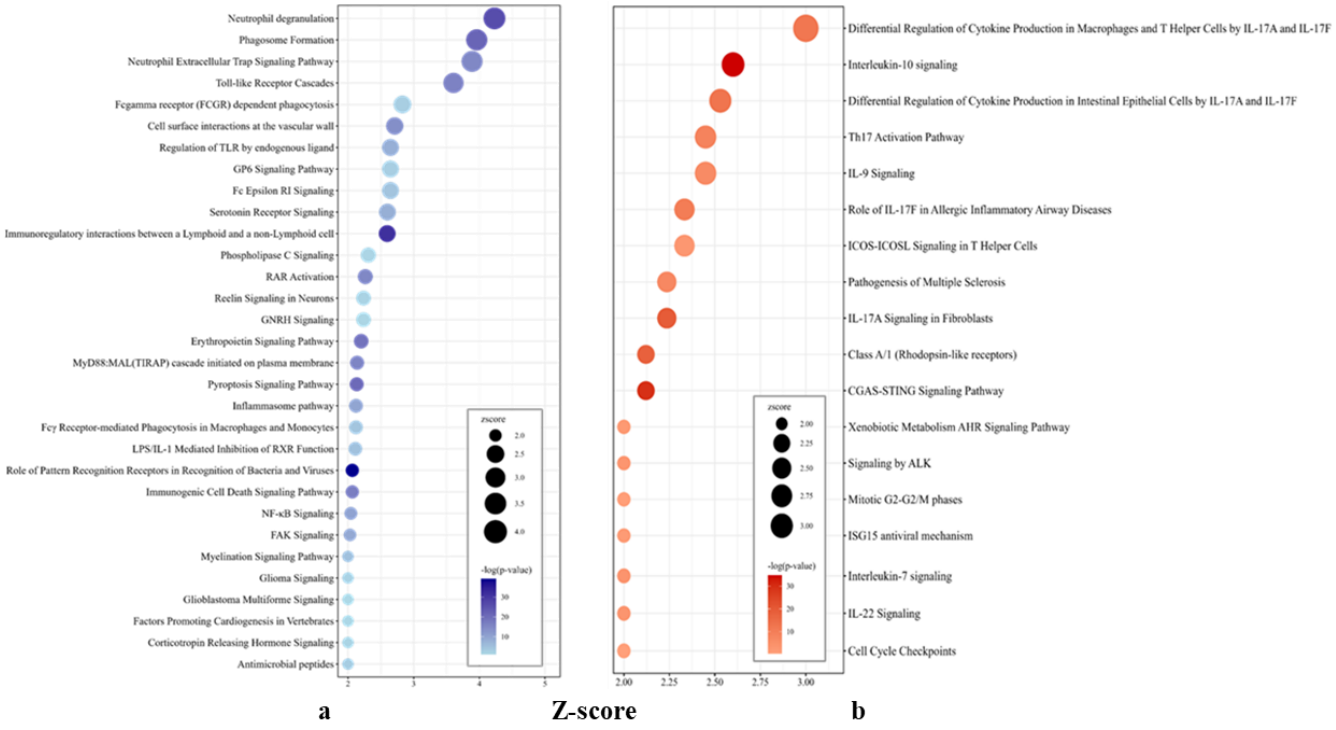

Figure 2. Dot plot of inhibited and activated canonical pathways (CPs) in VAX vs. T0.

The Ingenuity pathway analysis (IPA) analysis was performed on DEGs in VAX vs. T0, to identify inhibited (Z-score ≤ − 2) ***(a)*** *and activated (Z-score ≥ 2)* ***(b)*** *CPs. Pathways are displayed on the y-axis, while the x-axis represents the corresponding Z-score, which predicts the activation or inhibition state of biological pathways. Each dot corresponds to one pathway; dot size is proportional to the absolute Z-score, whereas dot color reflects statistical significance expressed as −log10(p-value). Only significantly enriched pathways are shown.*

The activation pathway profile observed in VAX vs. T0 delineates a cellular state characterized by strong immune activation, proliferation, and cytokine network engagement. The prominent activation of multiple CPs linked to Th17 (i.e., Differential Regulation of Cytokine Production in Macrophages and T Helper Cells by IL-17A and IL-17F, Differential Regulation of Cytokine Production in Intestinal Epithelial Cells by IL-17A and IL-17F, Th17 Activation Pathway, Role of IL-17F in Allergic inflammatory Airway Diseases, and IL-17A Signaling in Fibroblasts), reflects the induction of a type-17–oriented inflammatory program. The activation of interleukin-10 signaling further indicates the engagement of intrinsic negative feedback mechanisms. The activation of ICOS-ICOSL signaling, together with IL-7 and IL-9 signaling, indicates that vaccinating cells

have acquired a phenotype associated with T-cell survival. Importantly, cGAS-STING signaling and ISG15-mediated antiviral mechanisms are consistent with activation of innate nucleic-acid sensing and interferon-stimulated gene programs. The activation of mitotic G2-G2/M phase and cell-cycle checkpoint pathways reflects a highly proliferative cellular population maintaining control over replication-associated stress. The enrichment of xenobiotic metabolism and AHR signaling, together with Class A/1 (rhodopsin-like) receptor pathways, suggests engagement of chemotactic and trafficking programs. Downregulation of multiple pathways related to innate immune sensing, myeloid effector functions, and inflammatory cell death indicates a substantial attenuation of classical innate and myeloid-driven programs in VAX compared with T0. Several down-regulated pathways converge on TLR- and MyD88-dependent signaling, (i.e., Toll-like receptor cascades, MyD88:MAL (TIRAP) cascade initiated on plasma membrane, NF-κB signaling, and Role of Pattern Recognition Receptors in Recognition of Bacteria and Viruses). Together, these changes suggest reduced engagement of canonical pathogen-sensing and inflammatory transcriptional programs typically associated with monocytes and innate immune cells. In parallel, the down-regulation of inflammasome, pyroptosis, neutrophil extracellular trap formation, neutrophil degranulation, and antimicrobial peptide pathways points to suppression of highly inflammatory innate effector mechanisms. Consistent with this interpretation, pathways related to Fcγ receptor–mediated phagocytosis and phagosome formation are also down-regulated, indicating reduced representation or activation of professional phagocytic programs within the vaccine. Additional down-regulated pathways, including FAK signaling, cell surface interactions at the vascular wall, phospholipase C signaling, and GPCR-associated pathways, reflect attenuation of generalized adhesion, vascular interaction, and signaling modules.

4.2 Classification of DEGs in VAX vs. T0

To better characterize the differences of gene expression in VAX with respect to T0, statistically significant DEGs were subdivided into 25 classes. Each class comprises genes involved in specific biological processes, defined by grouping genes according to their functional roles in PBMC. The classes and the number of upregulated and downregulated genes are listed in Table 3.

Table 3. Classification of DEGs vs. T0

Biological Class	Total DEGs	Up-regulated DEGs	Down-regulated DEGs
Cytokines / growth factors and receptors	37	22 (59.5%)	15 (40.5%)
Adhesion and trafficking	33	12 (36.4%)	21 (63.6%)
Chemokine signaling and chemotaxis	31	24 (77.4%)	7 (22.6%)
Regulation of Inflammation	23	7 (30.4%)	16 (69.6%)
Transcription/signaling regulators	16	5 (31.3%)	11 (68.7%)
HLA Class I/II processing/presentation/autophagy	14	4 (28.6%)	10 (71.4%)
Type I_II_III IFN and IFN-responsive genes	14	10 (71.4%)	4 (28.6%)
T cell activation & differentiation	14	11 (78.6%)	3 (21.4%)
NK cytotoxicity	14	1 (7.1%)	13 (92.9%)
Co-stimulation	13	12 (92.3%)	1 (7.7%)
TNF	13	5 (38.5%)	8 (61.5%)
TLR system	13	1 (7.7%)	12 (92.3%)
Fc receptor / ADCC & phagocytosis	11	0 (0%)	11 (100%)
Basic cell function / housekeeping	11	8 (72.7%)	3 (27.3%)
Immune checkpoints	10	9 (90%)	1 (10%)
Complement system	10	5 (50%)	5 (50%)
Survival/Apoptosis/Proliferation	10	7 (70%)	3 (30%)
PRR C-type lectins & scavengers	9	2 (22.2%)	7 (77.8%)
CTA	9	9 (100%)	0 (0%)
B cell activation	5	2 (40%)	3 (60%)
Monocyte/DC phagocytosis & scavenging	5	1 (20%)	4 (80%)
Oxidative burst & antimicrobial factors	4	1 (25%)	3 (75%)
PRR - TLR pathway	3	1 (33.3%)	2 (66.7%)
TNF family signaling	2	2 (100%)	0 (0%)
Degranulation & granule effectors	2	2 (100%)	0 (0%)
Total	326		

The majority of DEGs belongs to the three classes: “Cytokines / growth factors and receptors”, “Chemokine signaling and chemotaxis” and “Adhesion and trafficking”.

4.3 Epigenetically-driven immunogenic properties of VAX

The epigenetically-driven immunogenic profile of VAX was assessed by comparison with the untreated condition, focusing on statistically significant DEGs associated with antigen presentation, costimulatory and co-inhibitory molecules, cross-priming, DC function, NK cytotoxicity and CTA.

The evaluation of the effect of decitabine on the functionality of the antigen presentation process was carried out by considering each VAX preparation individually. The results are shown in Figures 3, 4, and 5.

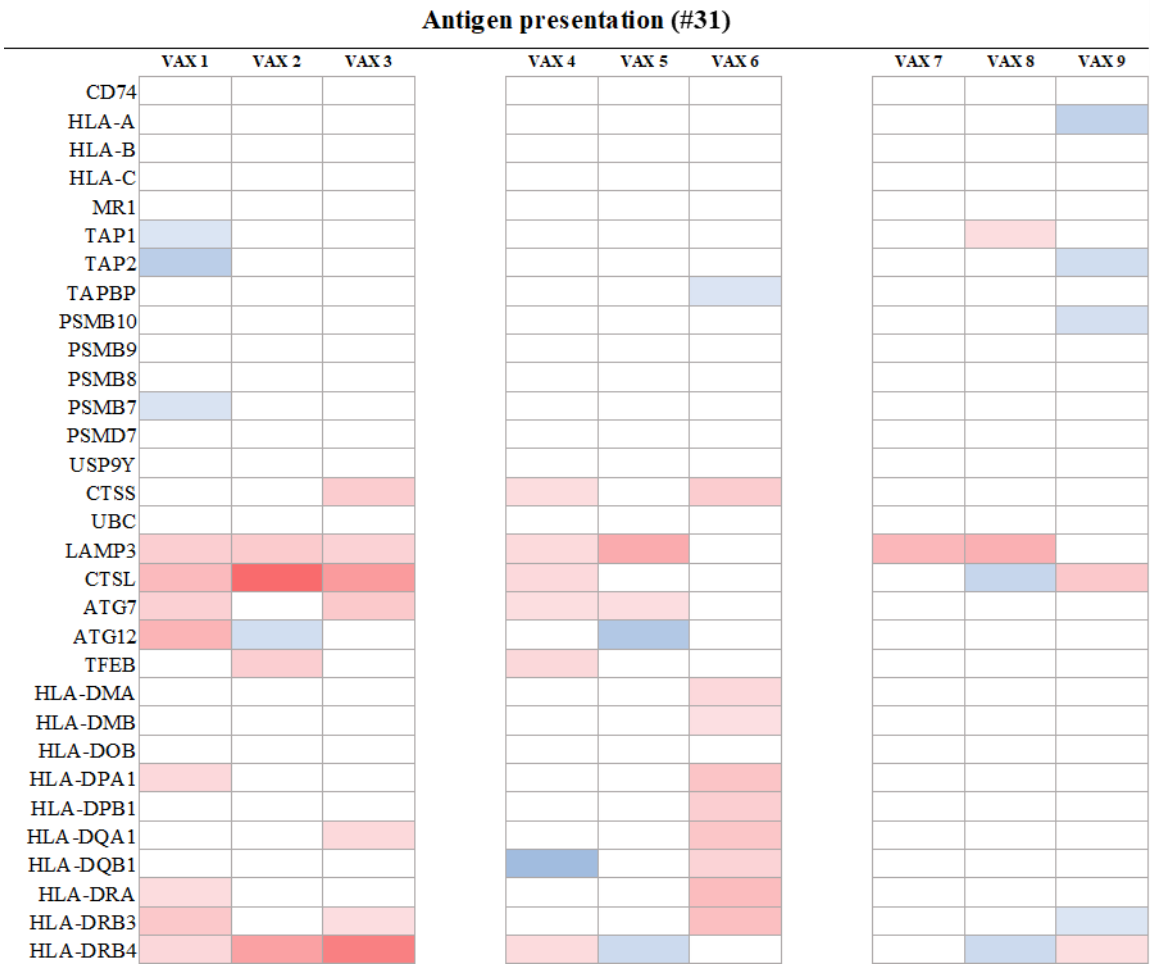

Figure 3. Heatmap illustrating the modulation of molecules involved in antigen processing and presentation after decitabine treatment.

Each gene is flanked by its fold change of expression (log2 fold change) observed in each VAX preparation (VAX 1-9). Genes with a log2 fold change ≥ 0.58 (FC = 1.5) were considered upregulated, whereas genes with a log2 fold change ≤ −0.58 (FC = −1.5) were considered downregulated. Genes were sorted in ascending order based on fold change values, which are represented by a color gradient ranging from intense red (log2 fold change = 5) to intense blue (log2 fold change = -5).

As shown in the figure, decitabine treatment exerted a limited modulatory effect on the expression of MHC class I and II molecules, the chaperone CD74, the non-classical MHC class I molecule MR1, the transporters TAP1 and TAP2, tapasin (TAPBP), genes associated with proteasome function (PSMB and PSMD), the ubiquitins USP9Y and UBC, and the protease CTSS. The lack of modulation may be explained by the high constitutive expression levels of these molecules. As shown in Figure 4, these genes exhibited high average count values across the VAX preparations, with the exception of HLA-DQA1 in VAX#3 and VAX#4, HLA-DQB1 in VAX#1, VAX#3, and VAX#4, HLA-DRB4 in VAX#2, VAX#3, VAX#5, and VAX#8, and USP9Y in VAX#3, VAX#7, and VAX#9. Notably, USP9Y was not expressed in these VAX preparations, as they were derived from female donors, and USP9Y is encoded on the Y chromosome.

In contrast, decitabine treatment showed the ability to upregulate the expression of LAMP3 and CTSL in the majority of the VAX preparations, as well as ATG7 in four preparations.

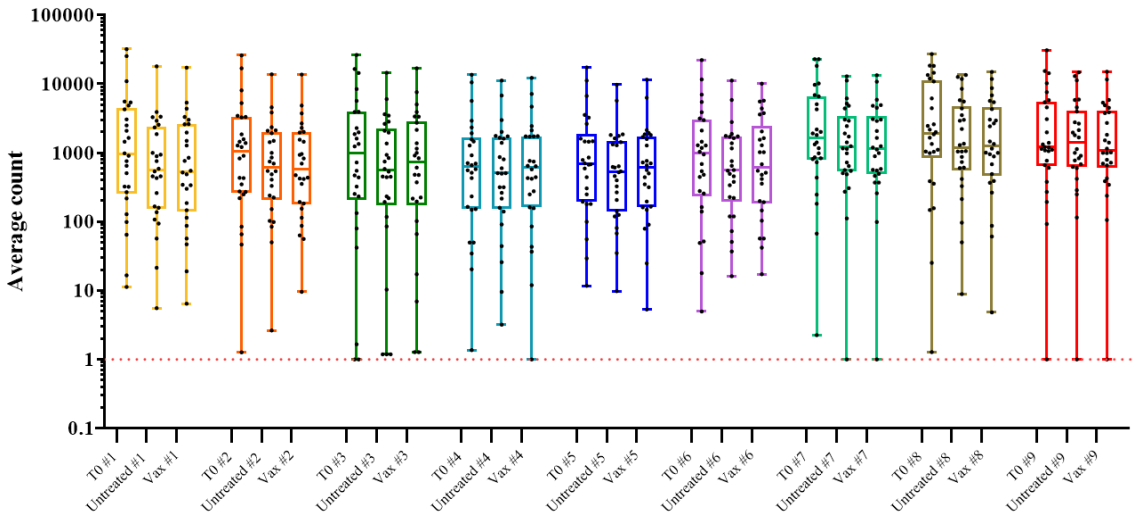

Figure 4. Box-and-whisker plot showing expression of MHC class I and II molecules and genes related to antigen-presenting machinery (APM) in T0, untreated and VAX samples.

Each gene is represented by a dot. Whiskers indicate minimum and maximum values, boxes represent lower and upper quartiles and the central line represent the median value. Gene expression levels are reported as average counts of mRNA molecules detected by nCounter Sprint Profiler and normalized to housekeeping genes included in the assay.

To further characterize the costimulatory potential of the vaccine following antigen presentation, the expression of genes involved in interactions with lymphocytes and dendritic cells was analyzed. As shown in Figure 5, each VAX preparation exhibited a distinct pattern of gene expression modulation following decitabine treatment. Nevertheless, upregulation of the costimulatory molecules TNFSF4, CD70, and ICOSLG was observed across all VAX preparations compared with the control untreated condition, while CD80 was upregulated in five preparations. Overall, decitabine treatment demonstrated the ability to enhance the expression of costimulatory molecules in most VAX preparations. In parallel, increased expression of the immune checkpoint molecules CD274 and CEACAM1 was observed in preparations derived from the first three donors, along with a marked upregulation of the majority of the immune checkpoints analyzed in VAX#8.

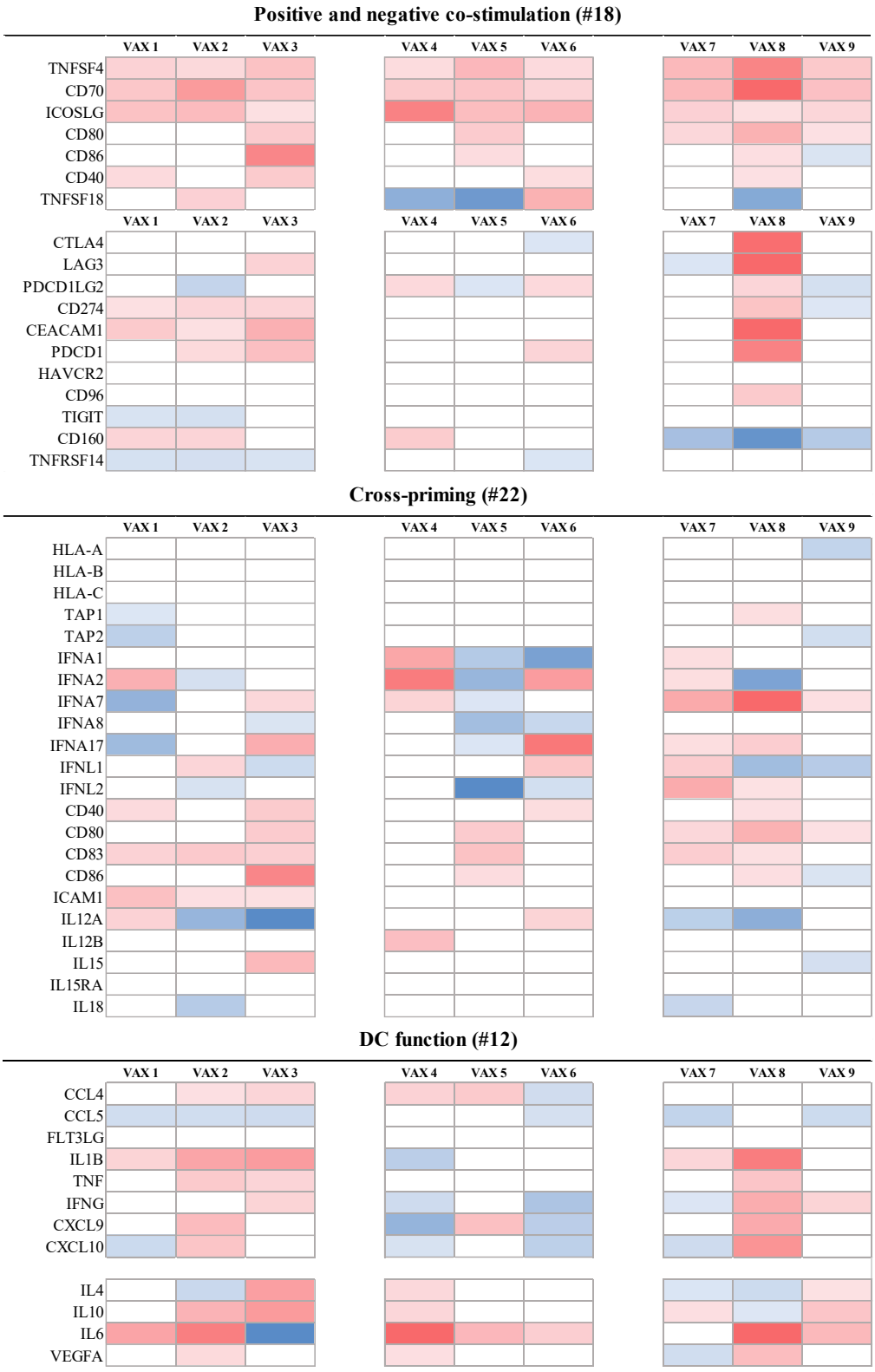

Figure 5. Heatmap illustrating the modulation of molecules involved in positive and negative co-stimulation, cross-priming and dendritic cells (DCs) function after decitabine treatment.

Each gene is flanked by its fold change of expression (log2 fold change) observed in each VAX preparation (VAX 1-9). Genes with a log2 fold change ≥ 0.58 (FC = 1.5) were considered upregulated, whereas genes with a log2 fold change ≤ −0.58 (FC = −1.5) were considered downregulated. Genes were sorted in ascending order based on fold change values, which are represented by a color gradient ranging from intense red (log2 fold change = 5) to intense blue (log2 fold change = -5).

Subsequently, the expression of genes representing activating and inhibitory signals for natural killer (NK) cells was evaluated. This analysis aimed to assess how decitabine treatment may affect the susceptibility of vaccine cells to NK cell–mediated cytotoxicity, which could potentially negatively impact vaccine functionality. As shown in Figure 6, decitabine treatment exerted a limited modulatory effect on the expression of triggering signals, primarily resulting in upregulation of the inhibitory signals CD274 and IL10.

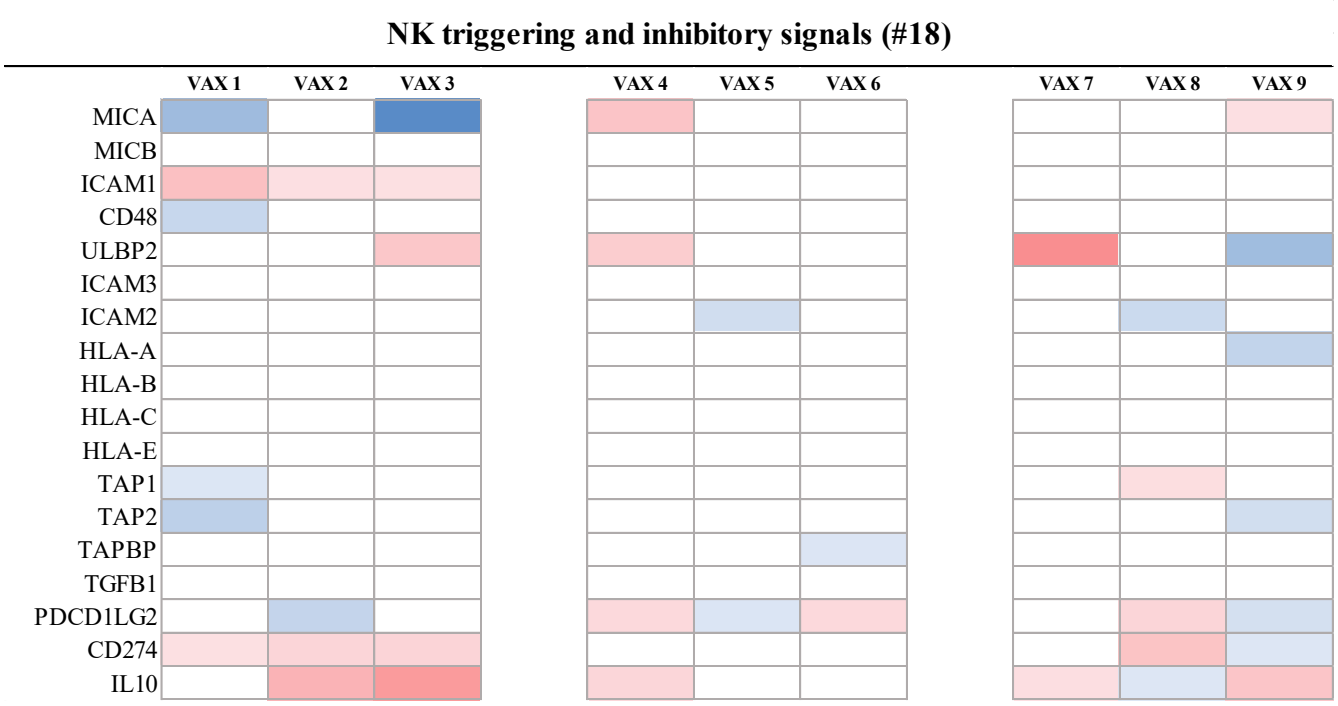

Figure 6. Heatmap illustrating the modulation of genes encoding activating and inhibitory signals for natural killer (NK) cells following decitabine treatment.

Each gene is flanked by its fold change of expression (log2 fold change) observed in each VAX preparation (VAX1-9). Genes with a log2 fold change ≥ 0.58 (FC = 1.5) were considered upregulated, whereas genes with a log2 fold change ≤ −0.58 (FC = −1.5) were considered downregulated. Genes were sorted in ascending order based on fold change values, which are represented by a color gradient ranging from intense red (log2 fold change = 5) to intense blue (log2 fold change = -5).

4.4 Analysis of CTA expression following decitabine treatment

Given the non-specific mechanism by which decitabine induces epigenetic remodeling, attention was also directed toward cancer–testis antigens (CTA) whose expression was assessed but did not reach statistical significance for differential expression. These data are shown in Figure 7.

A donor-specific upregulation profile was observed across the nine healthy donors. Indeed, when analyzed individually, each donor exhibited upregulation (log2 fold change ≥ 0.58) of a variable number of CTA, ranging from a minimum of 11 to a maximum of 22.

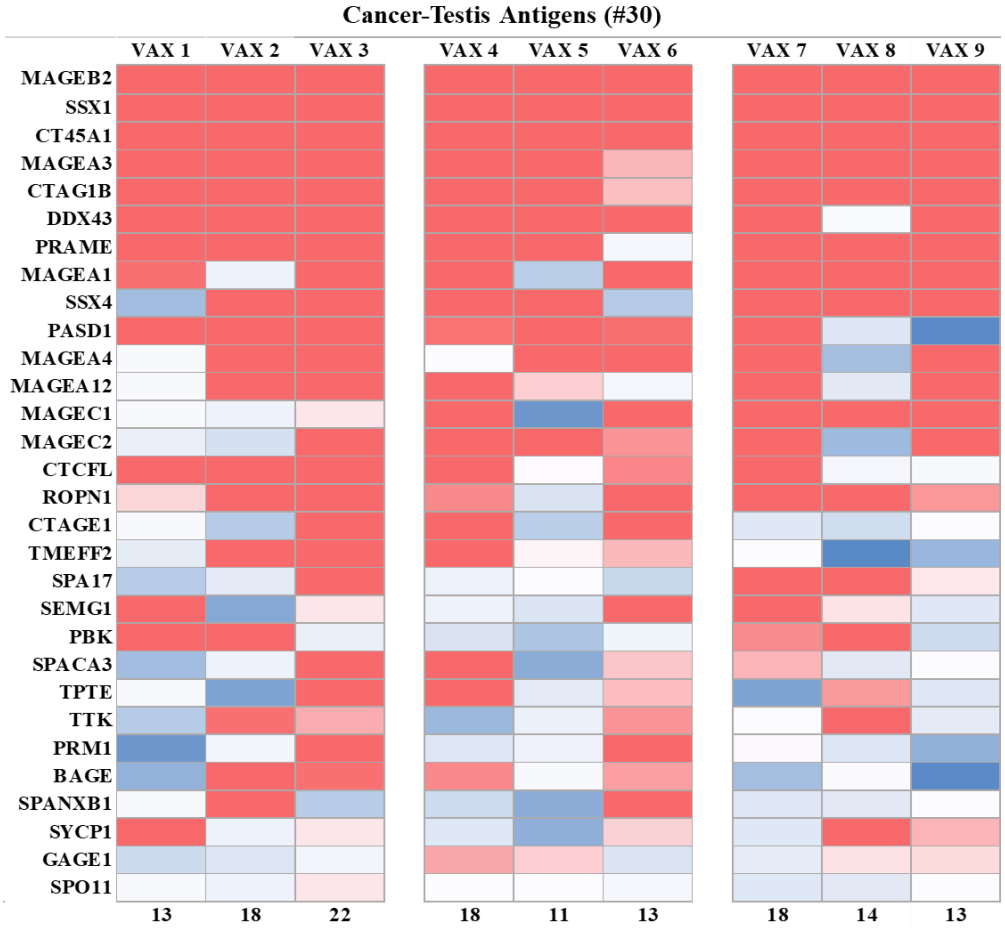

Figure 7. Heatmap illustrating modulation of CTA expression after decitabine treatment.

Each CTA is flanked by its fold change of expression (log2 fold change) observed in each VAX preparation (VAX 1-9). Genes with a log2 fold change ≥ 0.58 (FC = 1.5) were considered upregulated, whereas genes with a log2 fold change ≤ −0.58 (FC = −1.5) were considered downregulated. CTA were sorted in ascending order based on fold change values, which are represented by a color gradient ranging from intense red (maximum) to intense blue (minimum). The number of upregulated CTA is indicated below each VAX preparation.

4.5 Transposable element profiling

To further characterize the antigenic profile and immunogenic potential of VAX, RNA sequencing analyses were performed to evaluate the expression of TE. Figure 8 illustrates the TE modulated by decitabine treatment in VAX vs. untreated. Following decitabine exposure 1,626 TEs were found to be upregulated in VAX, whereas 80 TE were downregulated.

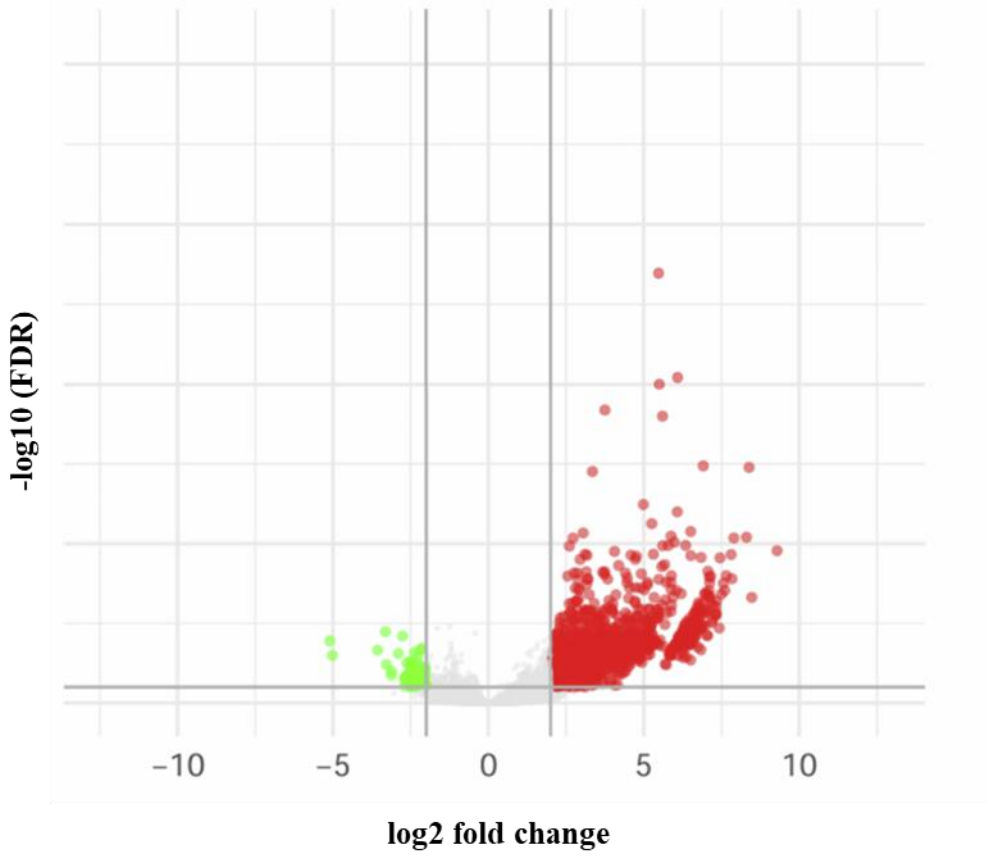

Figure 8. Volcano plot representing differentially expressed TE between VAX and untreated cells.

Each point corresponds to a TE, plotted according to its log2 fold change (x-axis) and statistical significance, expressed as the –log10 of the adjusted p-value (y-axis). After data normalization, differential TEs expression across experimental conditions was assessed using DESeq2. Genes with an adjusted p-value < 0.01 (Benjamini–Hochberg correction) and log2 fold change > 2 were considered differentially expressed. Significantly upregulated TEs are shown in red, while downregulated TEs are depicted in green.

The composition of upregulated TEs was subsequently analyzed and TE families and subfamilies are reported in Figure 9.

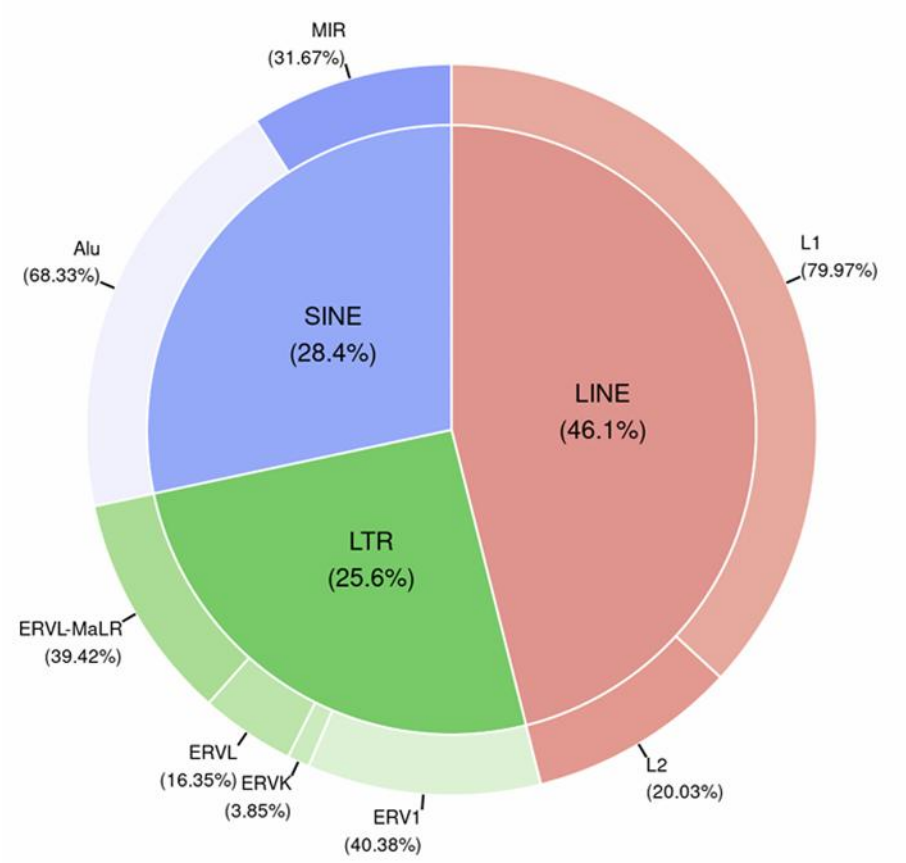

Figure 9. Pie chart representing families and subfamilies of upregulated TEs in VAX vs. untreated cells.

Major portions of the chart represent the three TE families SINE (blue), LINE (red) and LTR (green). SINE family is composed by Alu and MIR subfamilies, LINE by L1 and L2, and LTR by ERVL-MaLR, ERVL, ERVK, and ERV1.

The majority of upregulated TEs belonged to the non–long terminal repeat (non-LTR) families LINE (46.1%) and SINE (28.4%). Within the LINE family, the L1 subfamily was markedly more represented (79.97%) compared with L2 (20.03%). Among SINE elements, the Alu subfamily accounted for the largest proportion (68.33%). The remaining 25.6% of upregulated TEs belonged to the LTR family, within which the ERV1 and ERVL-MaLR subfamilies were the most represented (40.38% and 39.42%, respectively).

Furthermore, the genomic localization of upregulated TEs was determined to identify genes flanking each element. Enrichment analysis was subsequently performed on these flanking genes to characterize the potential impact of TE upregulation on gene expression. Figure 10 shows the biological pathways in which these genes are involved.

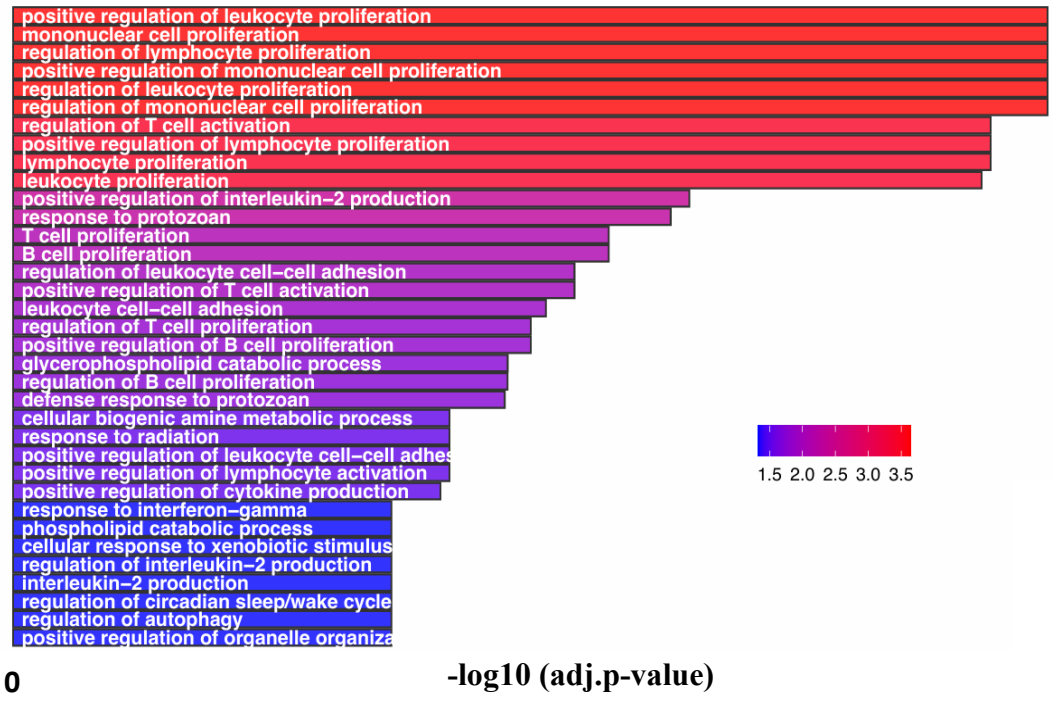

Figure 10. Enrichment analysis of genes flanking upregulated TE in VAX vs. untreated cells.

Flanking genes were identified based on the genomic localization of upregulated TE. Enrichment analysis was subsequently performed on the resulting gene set. Enriched pathways were ranked in descending order of statistical significance, expressed as −log10 of the adjusted p-value, and visualized using a color gradient ranging from blue (minimum) to red (maximum).

Enrichment analysis revealed that TEs upregulated by decitabine are most likely to impact biological processes related to leukocyte, mononuclear cell, and lymphocyte proliferation, as well as T-cell activation. Although with lower enrichment scores, TE upregulation was also found to significantly modulate pathways associated with cell adhesion, cytokine production, particularly interleukin-2 production, response to interferon-γ, and autophagy.

4.6 Characterization of miRNA expression profile

To investigate the modulation of miRNAs induced in VAX preparations, transcriptional analyses were performed using NanoString nCounter Sprint Profiler miRNA expression panel, on total RNA previously isolated from nine VAX, T0 and untreated cell preparations. Differentially expressed miRNAs (miRNA DE) were identified by comparing miRNA transcript counts in VAX samples with those in T0 and untreated conditions. The comparison between VAX and T0 identified #47 downregulated and #55 upregulated miRNAs (Figure 11).

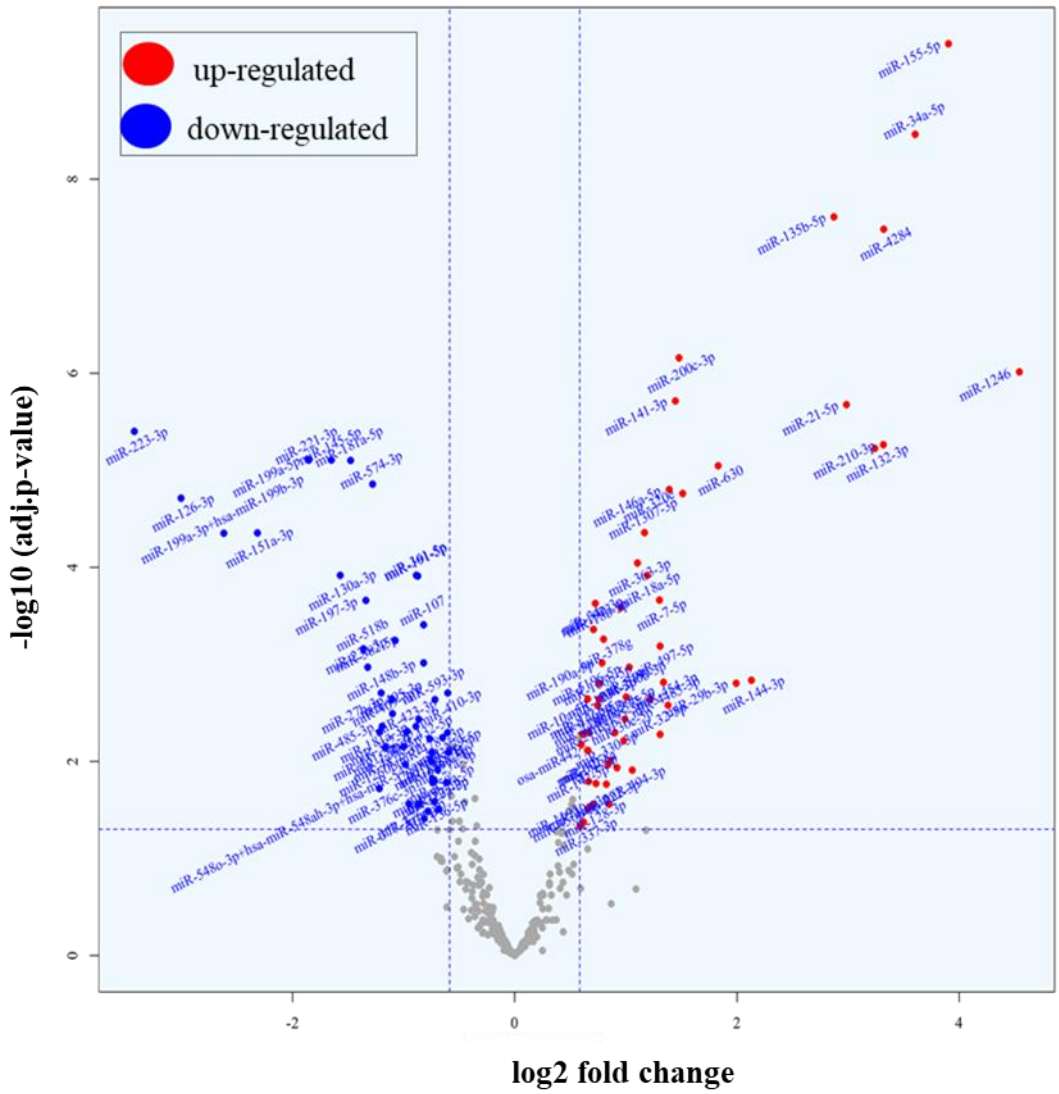

Figure 11. Volcano plot illustrating differentially expressed miRNAs (miRNA DE) between VAX and the original PBMC (T0).

Each point corresponds to a miRNA, plotted according to its log2 fold change (x-axis) and statistical significance, expressed as the –log10 of the adjusted p-value (y-axis). Differential expression analysis was performed using a two-sample t-test, followed by correction for multiple comparisons via the Benjamini-Hochberg false discovery rate (FDR) procedure. miRNAs with log2 fold change ≥ 0.58 (FC = 1.5) and an adjusted p-value corresponding to –log10(FDR) ≥ 1.3 (FDR ≤ 0.05) were considered upregulated. Whereas miRNAs with a log2 fold change ≤ -0.58 (FC = -1.5) and an adjusted p-value corresponding to –log10(FDR) ≥ 1.3 (FDR ≤ 0.05) were considered downregulated. Upregulated genes are shown in red, while downregulated genes are depicted in blue.

Among #47 miRNAs downregulated the ten most statistically significant downregulated miRNAs were hsa-miR-223-3p, hsa-miR-221-3p, hsa-miR-199a-5p, hsa-miR-145-5p, hsa-miR-181a-5p, hsa-miR-574-3p, hsa-miR-126-3p, hsa-miR-151a-3p, hsa-miR-199a-3p/hsa-miR-199b-3p, and hsa-miR-130a-3p (adjusted p-values from 3.96×10^{-06} to 1.20×10^{-04}). Conversely, the ten most statistically significant upregulated miRNAs among the 55 identified were hsa-miR-155-5p, hsa-miR-34a-5p, hsa-miR-135b-5p, hsa-miR-4284, hsa-miR-200c-3p, hsa-miR-1246, hsa-miR-141-3p, hsa-miR-21-5p, hsa-miR-210-3p, and hsa-miR-132-3p (adjusted p-values from 4.02×10^{-10} to 5.92×10^{-06}).

A subset of miRNAs, including hsa-miR-199a-3p and hsa-miR-199b-3p are reported as a single measurement because the mature 3p sequences are identical and cannot be discriminated by probe-based hybridization; therefore, the signal reflects the combined abundance of miR-199-3p species rather than locus-specific expression. Because hsa-miR-199a-3p and hsa-miR-199b-3p generate identical mature miRNA sequences, they are expected to exert overlapping biological functions by targeting the same mRNA repertoire; however, their transcription is controlled by distinct genomic loci and regulatory elements, which cannot be discriminated in probe-based NanoString assays.

To elucidate changes in miRNA expression, induced by epigenetic remodeling, miRNA transcript counts in VAX were compared with those detected in untreated cells. The results of the analysis are showed in Figure 12.

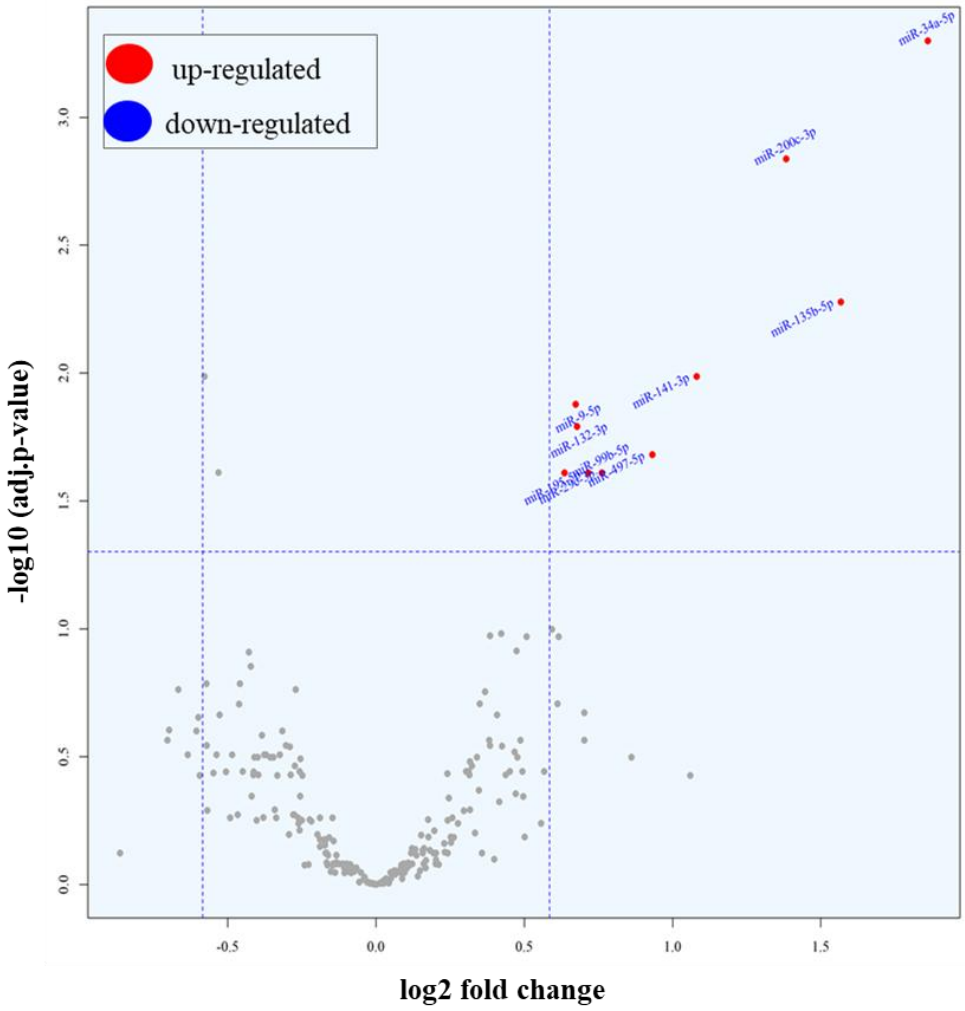

Figure 12. Volcano plot illustrating differentially expressed miRNAs (miRNA DE) between VAX and untreated conditions.

Each point corresponds to a miRNA, plotted according to its log2 fold change (x-axis) and statistical significance, expressed as the –log10 of the adjusted p-value (y-axis). Differential expression analysis was performed using a two-sample t-test, followed by correction for multiple comparisons via the Benjamini-Hochberg false discovery rate (FDR) procedure. miRNAs with log2 fold change ≥ 0.58 (FC = 1.5) and an adjusted p-value corresponding to –log10(FDR) ≥ 1.3 (FDR ≤ 0.05) were considered upregulated. Whereas miRNAs with a log2 fold change ≤ -0.58 (FC = -1.5) and an adjusted p-value corresponding to –log10(FDR) ≥ 1.3 (FDR ≤ 0.05) were considered downregulated. Significantly upregulated genes are shown in red, while downregulated genes are depicted in blue.

The analyses indicated that decitabine treatment in the nine VAX preparations did not result in statistically significant down-regulation of any of the miRNAs included in the panel. In contrast, a significant upregulation of ten miRNAs was observed, namely hsa-miR-34a-5p, hsa-miR-200c-3p, hsa-miR-135b-5p, hsa-miR-141-3p, hsa-miR-9-5p, hsa-miR-132-3p, hsa-miR-497-5p, hsa-miR-195-5p, hsa-miR-29c-3p, and hsa-miR-99b-5p, with adjusted p-values ranging from 5.02×10^{-04} to 2.46×10^{-02}.

4.7 Analyses of miRNA DE target genes

To assess the potential impact of significantly modulated miRNAs on gene expression in VAX, miRNA target genes were identified using miEAA 2.0. The analysis revealed that 47 miRNAs downregulated in VAX relative to T0 targeted 55 genes, whereas the 55 upregulated miRNAs targeted 289 genes. Additionally, the 10 miRNAs epigenetically upregulated in VAX compared with untreated samples targeted 367 genes.

To identify the biological pathways regulated by the target genes and consequently assess the potential biological impact of miRNAs modulated in VAX, an enrichment analysis was performed using the Enrichr software. Only pathways with a gene overlap of at least five genes and an adjusted p-value ≤ 0.05 were considered to be significantly impacted by the target genes of the modulated miRNAs. The analysis showed that miRNAs downregulated in VAX relative to T0 target genes involved in seven biological processes, whereas miRNAs upregulated in VAX relative to T0 and to untreated samples target genes involved in 203 and 72 biological processes, respectively. The top 20 enriched pathways, based on combined score, are showed in Figures 13 and 14.

Figure 13. Dot plot showing the top 20 Gene Ontology (GO) Biological Processes enriched among the predicted target genes of miRNAs upregulated in VAX compared with T0.

Enrichment analysis was performed using the Enrichr platform. Each dot represents a GO term; dot size corresponds to the Enrichr combined score, while color intensity reflects the adjusted p-value (FDR-corrected).

Compared with T0, VAX cells displayed upregulation of miRNAs whose predicted targets were predominantly associated with miRNA-related biological processes, namely Positive Regulation of miRNA Transcription (GO:1902895), Positive Regulation of miRNA Metabolic Process (GO:2000630), Regulation of miRNA Transcription (GO:1902893), and Positive Regulation of Transcription by RNA Polymerase II (GO:0045944). Within these pathways, upregulated miRNAs targeted a broad set of transcriptional, epigenetic, and signaling regulators, namely MYC, MYCN, MYB, E2F3, ETS1, KLF4, KLF5, SOX2, SOX12, GATA4, RUNX2, FOXP3, ZEB2, TCF7L1, JUN/FOS (AP-1), NFKB1, STAT3, HIF1A, SMAD2/3, NOTCH1/2, RBPJ, TGFB1, TGFB3, BMPR2, PIK3R1, PTEN, EGFR, VEGFA, TLR4, MAVS, IKBKB, TNFRSF1A, FADD, ATRX, TET1, UHRF1, SMARCA4, AUTS2, and RNF4. Moreover, upregulated miRNAs were associated with enrichment of the Extrinsic Apoptotic Signaling Pathway via Death Domain Receptors (GO:0008625) and the Extrinsic Apoptotic Signaling Pathway (GO:0097191), targeting TNFRSF10B, TNFRSF1A, FASLG, CASP8,

CASP8AP2, DAXX, BCL2, BCL2A1, SMAD3, TGFB1, and IL12A. In addition, upregulated miRNAs were associated with Cellular Response to Decreased Oxygen Levels (GO:0036294) and Cellular Response to Hypoxia (GO:0071456), by targeting key regulators such as NOTCH1, TGFB1, MYC, PTGS2, SIRT1, HIF1A, SIRT2, RTN4, MTOR, VEGFA, and CPEB4. Enrichr analysis further indicated that upregulated miRNAs were associated with enrichment of the Macrophage Differentiation pathway (GO:0030225) by targeting CDC42, CSF1R, CASP8, SOCS1, MMP9, SIRT1, and VEGFA. Conversely, the enrichment of Pulmonary Valve Development (GO:0003177), Aortic Valve Development (GO:0003176), Positive Regulation of Epithelial Cell Migration (GO:0010634), Ventricular Septum Development (GO:0003281), Positive Regulation of Epithelial to Mesenchymal Transition (GO:0010718), Negative Regulation of Fat Cell Differentiation (GO:0045599), Positive Regulation of Blood Vessel Endothelial Cell Migration (GO:0043536), Vasculogenesis (GO:0001570), Positive Regulation of Intracellular Signal Transduction (GO:1902533), Cellular Response to Mechanical Stimulus (GO:0071260) is likely driven by pleiotropic target genes annotated across multiple biological processes and should therefore be interpreted as non-specific in this context.

Compared with untreated, VAX cells displayed upregulation of miRNAs whose predicted targets are mainly involved in cellular cycle regulation, apoptosis, and survival (i.e., G1/S Transition of Mitotic Cell Cycle (GO:0000082), Positive Regulation of Mitotic Cell Cycle Phase Transition (GO:1901992), Cell Cycle G1/S Phase Transition (GO:0044843), Mitotic Cell Cycle Phase Transition (GO:0044772), Apoptotic Process (GO:0006915), and Negative Regulation of Programmed Cell Death (GO:0043069)). MiRNAs Target genes involved in these pathways were: the cyclin and CDKs CCND1/CCND3–CDK4/6, CCNE1/CCNE2, CCNA2, the phosphatases CDC25A/CDC25C, and the transcription factor E2F3, together with biosynthesis and survival regulators such as RPS6KB1 and BIRC5.

Besides, upregulated miRNAs were predicted to impact significantly on biological processes linked to autophagy/mitophagy (i.e., Mitophagy (GO:0000423), Autophagosome Assembly (GO:0000045), Autophagy of Mitochondrion (GO:0000422), and Autophagosome Maturation (GO:0097352)). Target genes within these biological pathways were the core autophagy/mitophagy regulators BECN1, ATG14, WIPI2, ATG5, GABARAPL1 and lysosomes-associated genes LAMP2 and CHMP4B.

Moreover, upregulated miRNAs in VAX cells preferentially target several transcriptional regulators including NOTCH2, JUN, SPI1, MYCN, SMAD3, MYB, KLF4, NFKB1, PPARA, and VEGFA that control Positive Regulation of miRNA Metabolic Process (GO:2000630), Regulation of miRNA Transcription (GO:1902893) and Positive Regulation of miRNA Transcription (GO:1902895).

Finally, as observed in the T0 comparison, the enrichment of the remaining biological processes (i.e., Wnt Signaling Pathway, Planar Cell Polarity Pathway (GO:0060071), Vasculogenesis (GO:0001570), Non-Canonical Wnt Signaling Pathway (GO:0035567), Regulation of Vascular Associated, Smooth Muscle Cell Proliferation (GO:1904705), and Positive Regulation of Epithelial to Mesenchymal Transition (GO:0010718)), in VAX vs. untreated cells, is difficult to interpret biologically and likely reflects non-specific overlap of pleiotropic genes that are annotated across multiple pathways.

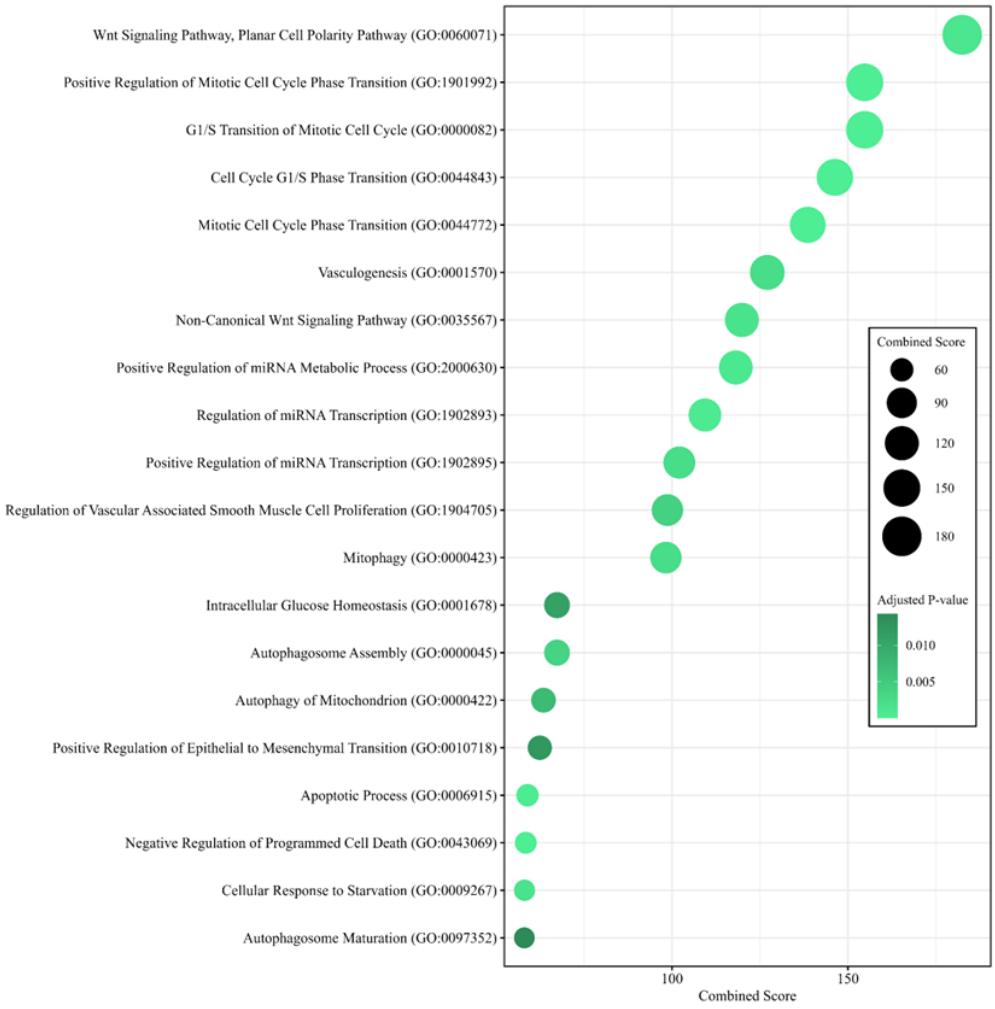

Figure 14. Dot plot showing the top 20 Gene Ontology (GO) Biological Processes enriched from the predicted target genes of miRNAs upregulated in VAX compared with untreated.

Enrichment analysis was performed using the Enrichr platform. Each dot represents a GO term; dot size corresponds to the Enrichr combined score, while color intensity reflects the adjusted p-value (FDR-corrected).

4.8 Functional validation of the epigenetically driven immunomodulatory properties of VAX

As functional validation of the epigenetic remodeling induced in the VAX immune profile, we investigated the immunomodulatory properties of the human cellular vaccine by analyzing the antigen-specific humoral immune response in a pre-clinical *in vivo* model. To this end, ELISA assays were performed on serum samples available from immunocompetent BALB/c mice repeatedly immunized with VAX or control (untreated) cells in a previous *in vivo* study. In detail, we assessed the presence of IgG antibodies specific for the human NY-ESO-1 protein in mouse sera collected on day 1 (pre-immunization) and on days 9, 16, and 23, corresponding to one week after the first, second, and third immunization, respectively.

Results, that are reported in Figure 15, showed that the antigen-specific antibody responses were induced in mice immunized with VAX following the second vaccination boost, compared with mice receiving untreated cells. Specifically, mice in the VAX group exhibited significantly higher levels of NY-ESO-1–specific

antibodies after the second immunization at serum dilutions of 1:50 (p = 0.001, mean FC = 2.2) and 1:100 (p = 0.008, mean FC = 1.9). A similar increase was observed after the third immunization, with significantly elevated antibody levels at 1:50 (p =0.1, mean FC = 1.8) and 1:100 (p = 0.1, mean FC = 1.8). In contrast, the untreated group displayed increased absorbance only at the lowest dilution (1:50), with a marked decrease at higher dilutions, suggesting non-specific antibody detection.

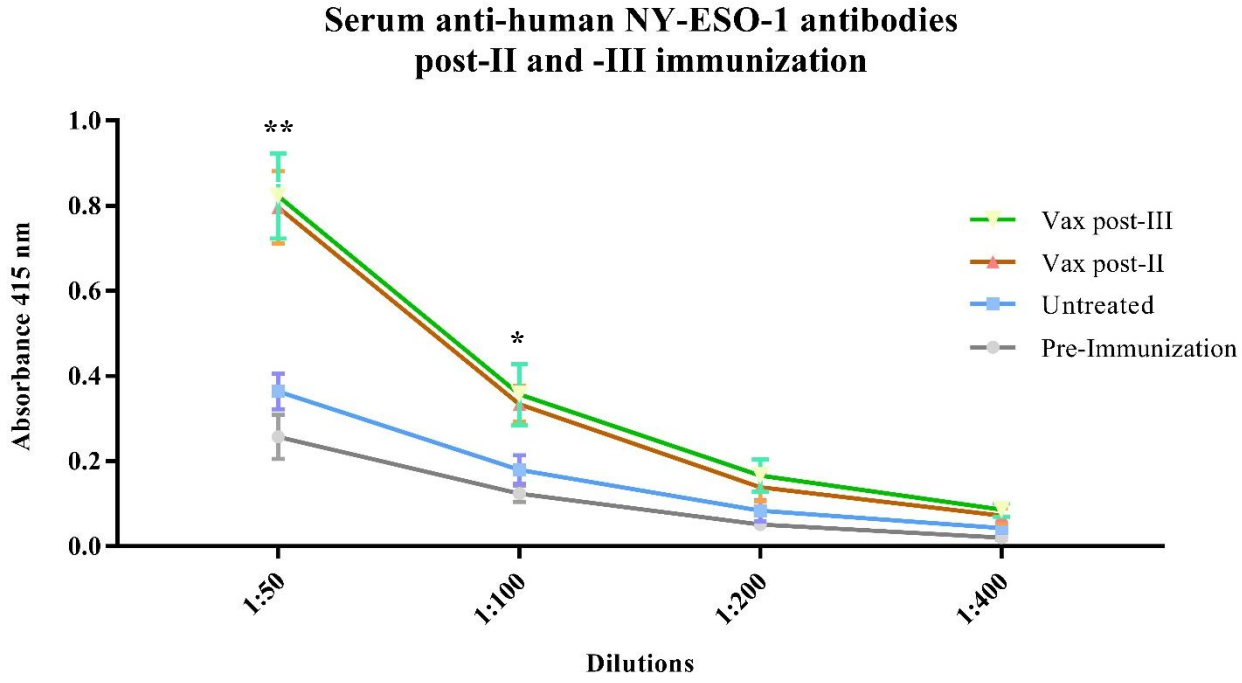

Figure 15. Serum antibody levels measured at different dilution factors after II (day 16) and III (days 23) VAX immunizations.

*Serum antibody levels were determined by ELISA using serial serum dilutions (1:50, 1:100, 1:200, and 1:400). Serum samples were collected from immunocompetent BALB/c mice immunized with VAX or untreated cells. Pre-immunization group consisted of mouse sera collected before treatment onset. Data are expressed as mean ± standard error of the mean. Absorbance was read by iMark™ Microplate Reader at 415 nm and normalized on the positive control (Origene mouse anti-human CTAG1B). ** p = 0.01, * p < 0.05 (unpaired t-test).*

5. DISCUSSION

In recent years, the development of anticancer vaccines capable of eliciting immune responses against a broad repertoire of tumor antigens has gained increasing attention. These therapeutic approaches have the potential to overcome resistance mechanisms associated with tumor heterogeneity and represent a promising strategy for patients who cannot benefit from currently available immunotherapeutic treatments. However, the need for tumor tissue as starting material, together with the time-consuming and costly manufacturing processes, currently limits their clinical applicability and restricts the number of patients who can be treated (Kaczmarek et al., 2023; Fan et al., 2023).

The aim of this project was to characterize an innovative vaccine platform capable of delivering a wide array of tumor antigens and adjuvant stimuli starting from a simple peripheral blood sample, through a rapid, scalable, and cost-effective process based on *ex vivo* mitogenic stimulation and epigenetic remodeling with decitabine. Specifically, we comprehensively characterized the transcriptional landscape shaped by the manufacturing process, examining both protein-coding genes and regulatory non-coding components, such as miRNAs and TE.

Overall, gene expression profiling revealed an activated pathway landscape in VAX compared with T0 cells, consistent with a vaccine product characterized by strong T-cell activation, proliferation, and cytokine network engagement, accompanied by innate immune sensing and immunoregulatory feedback mechanisms. Compared with the starting cellular population (T0), VAX preparations were enriched in lymphocyte-related biological processes. Notably, pathways related to IL-17, IL-7, IL-9, and IL-10 signaling were strongly activated in VAX, delineating pro-inflammatory profile associated with T cell survival and physiological counter-regulation in response to sustained immune activation (Ruiz De Morales et al., 2020; Kalim et al., 2024; ElKassar and Gress, 2010; Carlini et al., 2023).

In parallel the enrichment of mitotic G2–G2/M phase and cell-cycle checkpoint pathways indicates active cell proliferation. These findings are consistent with T-cell activation induced by OKT3 and the proliferative effects of IL-2 (Schwab et al., 1985). The combined action of these agents likely promoted selective activation and expansion of T-lymphocyte subsets within the initial PBMC population, with a proportional reduction of myeloid components, as indicated by the downregulation of pathways such as neutrophil degranulation, neutrophil extracellular trap formation, and Fcγ receptor–mediated phagocytosis.

Considering the stochastic nature of DNA demethylation and the intrinsic heterogeneity of the starting cellular populations, we performed donor-specific gene expression analyses to assess whether epigenetic remodeling activated shared immune-related pathways across individuals (Jakobsen et al., 2025).

Moreover, decitabine primarily acts on actively replicating cells, as it is incorporated into newly synthesized DNA strands during the S phase as a substrate of DNA polymerase α. Following stimulation with OKT3 and IL-2, the most actively proliferating cells are expected to be $CD3^+$ lymphocytes (Tovar et al., 1988). Consequently, decitabine had a limited impact on the expression of genes already activated by OKT3 and IL-2 in these cells, further reducing the number of differentially expressed genes observed between VAX and untreated samples.

In contrast, genes normally repressed by DNA methylation in PBMCs, such as cancer–testis antigens (CTA), displayed strong upregulation across all preparations. In the nine VAX preparations, upregulation was observed for a minimum of 11 and a maximum of 22 CTA among the 30 analyzed. Notably, the CTA MAGEB2, SSX1, CT45A1, MAGEA3, and CTAG1B (NY-ESO-1) were upregulated in all preparations. MAGEA3 and CTAG1B are overexpressed in various cancer types and play a crucial role in promoting cancer cell proliferation, migration, and metastasis (Thomas et al., 2018; Schäfer et al., 2021), thereby representing ideal targets for anticancer vaccination. Although MAGEB2, SSX1, and CT45A1 are less extensively studied than the former two CTA, their expression has been reported in multiple tumor types, and evidence suggests that their expression may confer a selective advantage to tumor cells (Peche et al., 2015; Alrubie et al., 2023; Meng et al., 2024). Furthermore, results from ELISA assays performed to detect anti–NY-ESO-1 IgG demonstrate that the protein is present in VAX and is expressed at levels sufficient to elicit a specific immune response *in vivo*. In addition, the epigenetic remodeling that led to the upregulation of numerous TE likely further expanded the antigenic repertoire in VAX. TE-derived neoantigens can arise as a consequence of epigenetic derepression, rendering them abundant and diverse in tumor cells. Notably, TE-derived neoantigens are generally absent in healthy tissues, and recent studies have demonstrated their immunogenic potential across multiple cancer types (Hu et al., 2024).

Moreover, the expression of MHC class I molecules, TAP transporters, proteasome components, and other antigen-processing proteins was already high under basal conditions. Consistent with this observation, the marked upregulation of TNFSF4 (OX40L), CD70, and ICOSLG indicates that VAX cells may not only passively deliver tumor antigens but also provide strong costimulatory signals to $CD8^+$ lymphocytes following antigen presentation on MHC molecules. Indeed, TNFSF4 acts as a costimulatory signal for T-cell activation, enhancing proliferation, survival, activation, and differentiation of $CD4^+$ and $CD8^+$ T cells, while also inhibiting the suppressive function of regulatory T cells (Deng et al., 2025, 2020; Kumar et al., 2019).

CD70 functions as a costimulatory ligand for CD27 expressed on most T lymphocytes. The CD70–CD27 pathway also plays a crucial role in promoting the differentiation of $CD8^+$ T cells into effector and memory lymphocytes, making it a key component in the amplification of cytotoxic T-cell responses against tumors (Hendriks et al., 2000; Keller et al., 2008; Van De Ven and Borst, 2015). Interactions between ICOS and ICOSL may also exert antitumor effects by increasing both $CD4^+ICOS^+$ and $CD8^+ICOS^+$ T cell subpopulations (Solinas et al., 2020).

Alongside the upregulation of these costimulatory molecules, decitabine treatment also induced, in some preparations, increased expression of CXCL9 and CXCL10, which attract $CD8^+$ T cells, thereby increasing the likelihood of their activation (Luri-Rey et al., 2025).

In addition to these costimulatory signals, the upregulation of CD80 and CD86 is of particular importance, as these molecules are essential for naïve T-cell priming. CD86 is generally expressed early during antigen-presenting cell activation and plays a prominent role in the initial priming of naïve T cells. Biophysical and functional studies have demonstrated that CD86 engages CD28 with rapid dynamic kinetics, favoring efficient costimulatory signaling during early APC-T cell interactions and effectively lowering the activation threshold

of naïve T cells. Moreover, CD86 displays reduced affinity for the inhibitory receptor CTLA-4 relative to CD80, resulting in preferential engagement of CD28 and enhanced activating costimulatory signaling during early T-cell priming (Linsley et al., 1994; Kennedy et al., 2022; Halliday et al., 2020).

In addition to promoting direct priming by VAX cells, our data also suggest the possibility of an indirect priming mechanism following antigen release into the microenvironment. The upregulation of molecules such as CCL4, IL-1B, and IFNG (IFN-γ) suggests that VAX may promote the recruitment and maturation of conventional type 1 dendritic cells (cDC1) (Luri-Rey et al., 2025), which excel at cross-presentation to activate antitumor $CD8^+$ T cells and also contribute to $CD4^+$ T cell priming (Heras-Murillo et al., 2025).

Nevertheless, *de novo* priming of tumor-specific $CD8^+$ T cells is critical for effective antitumor immunity, as intratumoral $CD8^+$ populations often become functionally exhausted. Therapeutic responses frequently depend on the recruitment of newly primed T cell clones, which can replace dysfunctional cells and broaden the antigenic repertoire targeted by the immune system (Yost et al., 2019; Palmeri et al., 2024; Giles et al., 2023; Wherry and Kurachi, 2015).

Our data also raise another important consideration regarding the potential of VAX to support immune responses against the delivered antigens, related to the ability of decitabine to upregulate the expression of MHC class II molecules, as well as the cysteine proteases CTSL and CTSS, which participate in antigen presentation by MHC class II molecules by regulating epitope generation and facilitating MHC II maturation (Hsieh et al., 2002), and LAMP3, which localizes to the MHC class II compartment of mature dendritic cells and is involved in the intracellular processing and trafficking of peptide-loaded MHC II molecules toward the cell surface (Salaun et al., 2004; Johansson et al., 2012).

Although our vaccine is primarily based on the presentation of intracellular antigens by cells that do not normally express MHC class II molecules, and only 10–30% of intracellular antigens are typically presented via these molecules (Blum et al., 2013). The upregulation of genes involved in this pathway could provide a complementary stimulus supporting antigen presentation to $CD4^+$ T cells in addition to $CD8^+$ T cells. Nevertheless, these observations must be interpreted with caution, as our analysis remains partial. Antigen presentation and T-cell priming are highly complex processes typically carried out by specialized cells that are not selectively expanded in VAX. Therefore, the molecular analyses performed in this project are not sufficient to determine whether, and how efficiently, these processes may occur when mediated by non-specialized cells. Moreover, some miRNAs upregulated by decitabine were found to target autophagy and mitophagy regulators (i.e., BECN1, ATG14, WIPI2, ATG5, GABARAPL1) and lysosome-associated genes (i.e., LAMP2 and CHMP4B). This adds an additional layer of uncertainty and variability within VAX preparations, as these processes are closely linked to the presentation of intracellular antigens on MHC class II molecules (Merkley et al., 2018; Blum et al., 2013).

Furthermore, based on our analyses, it is difficult to determine whether VAX can drive the differentiation of activated cells toward the acquisition of an effective antitumor effector phenotype. Although upregulation of type I and type III interferons was observed, the effects on IL-12, IL-15, and IL-18 expression were relatively modest. IL-12 bioactivities are important for TH1 differentiation and the acquisition of effector functions by

cytotoxic T lymphocytes, whereas the IL-15/IL-15Rα complex is recognized by IL-2Rβ–IL-2Rγ on T-cell surfaces, promoting activation and persistence of $CD8^+$ memory T cells. IL-18 synergizes with IL-12 to enhance IFN-γ production by T cells (Luri-Rey et al., 2025).

This observation could represent a limiting factor for the ability of VAX to directly promote the acquisition of antitumor effector functions by $CD8^+$ and $CD4^+$ T cells. However, it should be noted that these cytokines are primarily produced by dendritic cells, monocytes, or macrophages (Trinchieri, 2003; Waldmann, 2013), and their downregulation relative to T0 is therefore consistent with our culture protocol. Importantly, IL-15 and IL-18 mRNA levels remained detectable in VAX, and these cytokines are highly potent, exerting biological effects at very low concentrations (Wu et al., 2008; Ihim et al., 2022). IL-12A mRNA also remained detectable, whereas IL-12B did not, suggesting a functional loss of this cytokine in VAX, as IL-12A homodimers can bind IL-12R without exerting biological activity (Ling et al., 1995).

However, the expression of IL-12 and IL-15 is inducible *in vivo* by inflammatory signals including IFN-γ, TNF-α, IL-1β, and TLR ligands (Trinchieri, 2003). Notably, TNF-α, IL-1β, and TLR ligands, such as ERVs (Zhao et al., 2024), were upregulated by decitabine in VAX.

In addition, IL-1 can partially compensate for low IL-12 levels during $CD8^+$ T-cell priming by providing an alternative inflammatory "signal 3" that promotes clonal expansion and effector differentiation, although IL-12 remains critical for optimal Th1 imprinting and long-term memory formation (Curtsinger and Mescher, 2010).

Finally, the increase in immune checkpoints involved in the effector phase of the immune response (e.g., PD-1 (PDCD1), LAG3, and TIM3 (HAVCR2)), together with IL-10 upregulation, indicates the presence of a physiological brake on activation. This suggests potentially limited *in vivo* side effects of VAX, which may offer advantages, including compatibility with combination therapies. However, the increase in PD-L1/2 (CD274/PDCD1LG2) and CTLA-4 expression may lead, both directly and indirectly, to attenuated priming (Zhao et al., 2018; Soskic et al., 2021).

This observation should be interpreted in light of the fact that epigenetic remodeling in VAX induced the expression of both CD80/CD86 and PD-L1/L2 ligands (De Vos et al., 2020) in activated and proliferating cells, in which activation likely also induced CTLA-4 and PD-1 expression (Rowshanravan et al., 2018; Patsoukis et al., 2020). This may result in cells co-expressing these checkpoints and their ligands.

It has been demonstrated that co-expressed PD-1 interacts *in cis* with both PD-L1 and PD-L2 on cell membranes. Such interaction inhibits the ability of PD-L1 to bind T-cell-intrinsic PD-1 in trans, thereby repressing canonical PD-L1/PD-1 inhibitory signaling (Zhao et al., 2018). Furthermore, recent data revealed that CD80 physically interacts with PD-L1 in cis, preventing its binding to PD-1 (Kennedy et al., 2022). Similarly, evidence suggests that CD80 may also interact in cis with CTLA-4, inhibiting its function and preventing attenuation of the priming process. Moreover, the significant upregulation of miR-34a-5p, which targets FOXP3, suggests that VAX may contribute to reducing the regulatory T cell (Treg) population (Xie et al., 2019). A decrease in Treg cells could, in turn, attenuate their suppressive effects on CD80 and CD86-mediated costimulatory signaling, thereby enhancing the intensity of the immune response.

Comprehensively, these findings are encouraging for the clinical application of VAX. In fact, our data suggest that, despite the variability observed among different preparations, VAX cells collectively express a broad set of immunogenic antigens and molecules capable of providing co-stimulation and priming of $CD8^+$ T cells, and $CD4^+$ T cells. This is complemented by cytokines capable of directing lymphocyte differentiation toward an antitumor phenotype, either directly or through interactions with the microenvironment.

6. REFERENCES

Ai, H., Yang, H., Li, L., Ma, J., Liu, K., Li, Z., 2023. Cancer/testis antigens: promising immunotherapy targets for digestive tract cancers. Front. Immunol. 14, 1190883. https://doi.org/10.3389/fimmu.2023.1190883

Alrubie, T.M., Alamri, A.M., Almutairi, B.O., Alrefaei, A.F., Arafah, M.M., Alanazi, M., Semlali, A., Almutairi, M.H., 2023. Higher Expression Levels of SSX1 and SSX2 in Patients with Colon Cancer: Regulated In Vitro by the Inhibition of Methylation and Histone Deacetylation. Medicina (Mex.) 59, 988. https://doi.org/10.3390/medicina59050988

Angeloni, A., Bogdanovic, O., 2021. Sequence determinants, function, and evolution of CpG islands. Biochem. Soc. Trans. 49, 1109–1119. https://doi.org/10.1042/BST20200695

Aparicio-Puerta, E., Hirsch, P., Schmartz, G.P., Kern, F., Fehlmann, T., Keller, A., 2023. miEAA 2023: updates, new functional microRNA sets and improved enrichment visualizations. Nucleic Acids Res. 51, W319–W325. https://doi.org/10.1093/nar/gkad392

Bastin, D.J., Montroy, J., Kennedy, M.A., Martel, A.B., Shorr, R., Ghiasi, M., Boucher, D.M., Wong, B., Gresham, L., Diallo, J.-S., Fergusson, D.A., Lalu, M.M., Kekre, N., Auer, R.C., 2023. Safety and efficacy of autologous cell vaccines in solid tumors: a systematic review and meta-analysis of randomized control trials. Sci. Rep. 13, 3347. https://doi.org/10.1038/s41598-023-29630-9

Blum, J.S., Wearsch, P.A., Cresswell, P., 2013. Pathways of Antigen Processing. Annu. Rev. Immunol. 31, 443–473. https://doi.org/10.1146/annurev-immunol-032712-095910

Buonaguro, L., Tagliamonte, M., 2020. Selecting Target Antigens for Cancer Vaccine Development. Vaccines 8, 615. https://doi.org/10.3390/vaccines8040615

Carlini, V., Noonan, D.M., Abdalalem, E., Goletti, D., Sansone, C., Calabrone, L., Albini, A., 2023. The multifaceted nature of IL-10: regulation, role in immunological homeostasis and its relevance to cancer, COVID-19 and post-COVID conditions. Front. Immunol. 14, 1161067. https://doi.org/10.3389/fimmu.2023.1161067

Chekaoui, A., Garofalo, M., Gad, B., Staniszewska, M., Chiaro, J., Pancer, K., Gryciuk, A., Cerullo, V., Salmaso, S., Caliceti, P., Masny, A., Wieczorek, M., Pesonen, S., Kuryk, L., 2024. Cancer vaccines: an update on recent achievements and prospects for cancer therapy. Clin. Exp. Med. 25, 24. https://doi.org/10.1007/s10238-024-01541-7

Chen, E.Y., Tan, C.M., Kou, Y., Duan, Q., Wang, Z., Meirelles, G.V., Clark, N.R., Ma'ayan, A., 2013. Enrichr: interactive and collaborative HTML5 gene list enrichment analysis tool. BMC Bioinformatics 14, 128. https://doi.org/10.1186/1471-2105-14-128

Curtsinger, J.M., Mescher, M.F., 2010. Inflammatory cytokines as a third signal for T cell activation. Curr. Opin. Immunol. 22, 333–340. https://doi.org/10.1016/j.coi.2010.02.013

Dai, W., Qiao, X., Fang, Y., Guo, R., Bai, P., Liu, S., Li, T., Jiang, Y., Wei, S., Na, Z., Xiao, X., Li, D., 2024. Epigenetics-targeted drugs: current paradigms and future challenges. Signal Transduct. Target. Ther. 9, 332. https://doi.org/10.1038/s41392-024-02039-0

De Vos, L., Grünwald, I., Bawden, E.G., Dietrich, J., Scheckenbach, K., Wiek, C., Zarbl, R., Bootz, F., Landsberg, J., Dietrich, D., 2020. The landscape of CD28, CD80, CD86, CTLA4, and ICOS DNA methylation in head and neck squamous cell carcinomas. Epigenetics 15, 1195–1212. https://doi.org/10.1080/15592294.2020.1754675

Deng, T., Suo, C., Chang, J., Yang, R., Li, J., Cai, T., Qiu, J., 2020. ILC3-derived OX40L is essential for homeostasis of intestinal Tregs in immunodeficient mice. Cell. Mol. Immunol. 17, 163–177. https://doi.org/10.1038/s41423-019-0200-x

Deng, Z., Li, L., Meng, Z., Zeng, G., Cao, R., Liu, R., 2025. Pan-cancer analysis shows that TNFSF4 is a potential prognostic and immunotherapeutic biomarker for multiple cancer types including liver cancer. BMC Cancer 25, 100. https://doi.org/10.1186/s12885-025-13479-4

Dhillon, P., Mulholland, K.A., Hu, H., Park, J., Sheng, X., Abedini, A., Liu, H., Vassalotti, A., Wu, J., Susztak, K., 2023. Increased levels of endogenous retroviruses trigger fibroinflammation and play a role in kidney disease development. Nat. Commun. 14, 559. https://doi.org/10.1038/s41467-023-36212-w

Dobin, A., Davis, C.A., Schlesinger, F., Drenkow, J., Zaleski, C., Jha, S., Batut, P., Chaisson, M., Gingeras, T.R., 2013. STAR: ultrafast universal RNA-seq aligner. Bioinformatics 29, 15–21. https://doi.org/10.1093/bioinformatics/bts635

ElKassar, N., Gress, R.E., 2010. An overview of IL-7 biology and its use in immunotherapy. J. Immunotoxicol. 7, 1–7. https://doi.org/10.3109/15476910903453296

Fan, T., Zhang, M., Yang, J., Zhu, Z., Cao, W., Dong, C., 2023. Therapeutic cancer vaccines: advancements, challenges and prospects. Signal Transduct. Target. Ther. 8, 450. https://doi.org/10.1038/s41392-023-01674-3

Fazio, C., Covre, A., Cutaia, O., Lofiego, M.F., Tunici, P., Chiarucci, C., Cannito, S., Giacobini, G., Lowder, J.N., Ferraldeschi, R., Taverna, P., Di Giacomo, A.M., Coral, S., Maio, M., 2018. Immunomodulatory Properties of DNA Hypomethylating Agents: Selecting the Optimal Epigenetic Partner for Cancer Immunotherapy. Front. Pharmacol. 9, 1443. https://doi.org/10.3389/fphar.2018.01443

Fuso, A., Raia, T., Orticello, M., Lucarelli, M., 2020. The complex interplay between DNA methylation and miRNAs in gene expression regulation. Biochimie 173, 12–16. https://doi.org/10.1016/j.biochi.2020.02.006

Garde, C., Pavlidis, M.A., Garces, P., Lange, E.J., Ramarathinam, S.H., Sokač, M., Pandey, K., Faridi, P., Ahrenfeldt, J., Chung, S., Friis, S., Kleine-Kohlbrecher, D., Birkbak, N.J., Kringelum, J.V., Rønø, B., Purcell, A.W., Trolle, T., 2025. Endogenous viral elements constitute a complementary source of antigens for personalized cancer vaccines. Npj Vaccines 10, 54. https://doi.org/10.1038/s41541-025-01107-y

Gibney, E.R., Nolan, C.M., 2010. Epigenetics and gene expression. Heredity 105, 4–13. https://doi.org/10.1038/hdy.2010.54

Giles, J.R., Globig, A.-M., Kaech, S.M., Wherry, E.J., 2023. CD8+ T cells in the cancer-immunity cycle. Immunity 56, 2231–2253. https://doi.org/10.1016/j.immuni.2023.09.005

Glaich, O., Parikh, S., Bell, R.E., Mekahel, K., Donyo, M., Leader, Y., Shayevitch, R., Sheinboim, D., Yannai, S., Hollander, D., Melamed, Z., Lev-Maor, G., Ast, G., Levy, C., 2019. DNA methylation directs microRNA biogenesis in mammalian cells. Nat. Commun. 10, 5657. https://doi.org/10.1038/s41467-019-13527-1

Guan, H., Wu, Y., Li, L., Yang, Y., Qiu, S., Zhao, Z., Chu, X., He, J., Chen, Z., Zhang, Y., Ding, H., Pan, J., Pan, Y., 2023. Tumor neoantigens: Novel strategies for application of cancer immunotherapy. Oncol. Res. 31, 437–448. https://doi.org/10.32604/or.2023.029924

Halliday, N., Williams, C., Kennedy, A., Waters, E., Pesenacker, A.M., Soskic, B., Hinze, C., Hou, T.Z., Rowshanravan, B., Janman, D., Walker, L.S.K., Sansom, D.M., 2020. CD86 Is a Selective CD28 Ligand Supporting FoxP3+ Regulatory T Cell Homeostasis in the Presence of High Levels of CTLA-4. Front. Immunol. 11, 600000. https://doi.org/10.3389/fimmu.2020.600000

Hegoburu, A., Amer, M., Frizelle, F., Purcell, R., 2025. B cells and tertiary lymphoid structures in cancer therapy response. BJC Rep. 3, 40. https://doi.org/10.1038/s44276-025-00146-1

Hendriks, J., Gravestein, L.A., Tesselaar, K., Van Lier, R.A.W., Schumacher, T.N.M., Borst, J., 2000. CD27 is required for generation and long-term maintenance of T cell immunity. Nat. Immunol. 1, 433–440. https://doi.org/10.1038/80877

Heras-Murillo, I., Mañanes, D., Munné, P., Núñez, V., Herrera, J., Catalá-Montoro, M., Alvarez, M., Del Pozo, M.A., Melero, I., Wculek, S.K., Sancho, D., 2025. Immunotherapy with conventional type-1 dendritic cells induces immune memory and limits tumor relapse. Nat. Commun. 16, 3369. https://doi.org/10.1038/s41467-025-58289-1

Hollingsworth, R.E., Jansen, K., 2019. Turning the corner on therapeutic cancer vaccines. Npj Vaccines 4, 7. https://doi.org/10.1038/s41541-019-0103-y

Hsieh, C.-S., deRoos, P., Honey, K., Beers, C., Rudensky, A.Y., 2002. A Role for Cathepsin L and Cathepsin S in Peptide Generation for MHC Class II Presentation. J. Immunol. 168, 2618–2625. https://doi.org/10.4049/jimmunol.168.6.2618

Hu, Z., Guo, X., Li, Z., Meng, Z., Huang, S., 2024. The neoantigens derived from transposable elements – A hidden treasure for cancer immunotherapy. Biochim. Biophys. Acta BBA - Rev. Cancer 1879, 189126. https://doi.org/10.1016/j.bbcan.2024.189126

Ihim, S.A., Abubakar, S.D., Zian, Z., Sasaki, T., Saffarioun, M., Maleknia, S., Azizi, G., 2022. Interleukin-18 cytokine in immunity, inflammation, and autoimmunity: Biological role in induction, regulation, and treatment. Front. Immunol. 13, 919973. https://doi.org/10.3389/fimmu.2022.919973

Jakobsen, M.K., Traynor, S., Nielsen, A.Y., Dahl, C., Staehr, M., Jakobsen, S.T., Madsen, M.S., Siersbaek, R., Terp, M.G., Jensen, J.B., Pedersen, C.B., Shrestha, A., Brewer, J.R., Duijf, P.H.G., Gammelgaard, O.L., Ditzel, H.J., Kirkin, A.F., Guldberg, P., Gjerstorff, M.F., 2025. Stochastic demethylation and redundant epigenetic suppressive mechanisms generate highly heterogeneous responses to pharmacological DNA methyltransferase inhibition. J. Exp. Clin. Cancer Res. 44, 21. https://doi.org/10.1186/s13046-025-03294-x

Johansson, P., Corripio-Miyar, Y., Wang, T., Collet, B., Secombes, C.J., Zou, J., 2012. Characterisation and expression analysis of the rainbow trout (Oncorhynchus mykiss) homologue of the human dendritic cell marker CD208/lysosomal associated membrane protein 3. Dev. Comp. Immunol. 37, 402–413. https://doi.org/10.1016/j.dci.2012.02.012

Kaczmarek, M., Poznańska, J., Fechner, F., Michalska, N., Paszkowska, S., Napierała, A., Mackiewicz, A., 2023. Cancer Vaccine Therapeutics: Limitations and Effectiveness—A Literature Review. Cells 12, 2159. https://doi.org/10.3390/cells12172159

Kalim, M., Jing, R., Guo, W., Xing, H., Lu, Y., 2024. Functional diversity and regulation of IL-9-producing T cells in cancer immunotherapy. Cancer Lett. 606, 217306. https://doi.org/10.1016/j.canlet.2024.217306

Kamath, V., 2021. Cancer vaccines: An unkept promise? Drug Discov. Today 26, 1347–1352. https://doi.org/10.1016/j.drudis.2021.02.006

Keller, A.M., Schildknecht, A., Xiao, Y., Van Den Broek, M., Borst, J., 2008. Expression of Costimulatory Ligand CD70 on Steady-State Dendritic Cells Breaks CD8+ T Cell Tolerance and Permits Effective Immunity. Immunity 29, 934–946. https://doi.org/10.1016/j.immuni.2008.10.009

Kennedy, A., Waters, E., Rowshanravan, B., Hinze, C., Williams, C., Janman, D., Fox, T.A., Booth, C., Pesenacker, A.M., Halliday, N., Soskic, B., Kaur, S., Qureshi, O.S., Morris, E.C., Ikemizu, S., Paluch, C., Huo, J., Davis, S.J., Boucrot, E., Walker, L.S.K., Sansom, D.M., 2022. Differences in CD80 and CD86 transendocytosis reveal CD86 as a key target for CTLA-4 immune regulation. Nat. Immunol. 23, 1365–1378. https://doi.org/10.1038/s41590-022-01289-w

Kong, Y., Rose, C.M., Cass, A.A., Williams, A.G., Darwish, M., Lianoglou, S., Haverty, P.M., Tong, A.-J., Blanchette, C., Albert, M.L., Mellman, I., Bourgon, R., Greally, J., Jhunjhunwala, S., Chen-Harris, H., 2019. Transposable element expression in tumors is associated with immune infiltration and increased antigenicity. Nat. Commun. 10, 5228. https://doi.org/10.1038/s41467-019-13035-2

Krämer, A., Green, J., Pollard, J., Tugendreich, S., 2014. Causal analysis approaches in Ingenuity Pathway Analysis. Bioinformatics 30, 523–530. https://doi.org/10.1093/bioinformatics/btt703

Kuleshov, M.V., Jones, M.R., Rouillard, A.D., Fernandez, N.F., Duan, Q., Wang, Z., Koplev, S., Jenkins, S.L., Jagodnik, K.M., Lachmann, A., McDermott, M.G., Monteiro, C.D., Gundersen, G.W., Ma'ayan, A., 2016. Enrichr: a comprehensive gene set enrichment analysis web server 2016 update. Nucleic Acids Res. 44, W90-97. https://doi.org/10.1093/nar/gkw377

Kumar, P., Marinelarena, A., Raghunathan, D., Ragothaman, V.K., Saini, S., Bhattacharya, P., Fan, J., Epstein, A.L., Maker, A.V., Prabhakar, B.S., 2019. Critical role of OX40 signaling in the TCR-independent phase of human and murine thymic Treg generation. Cell. Mol. Immunol. 16, 138–153. https://doi.org/10.1038/cmi.2018.8

Lanciano, S., Cristofari, G., 2024. Cancer Immunotherapy: How to Exploit Transposable Elements? Clin. Chem. 70, 17–20. https://doi.org/10.1093/clinchem/hvad091

Lee, K.-W., Yam, J.W.P., Mao, X., 2023. Dendritic Cell Vaccines: A Shift from Conventional Approach to New Generations. Cells 12, 2147. https://doi.org/10.3390/cells12172147

Liang, Y., Qu, X., Shah, N.M., Wang, T., 2024. Towards targeting transposable elements for cancer therapy. Nat. Rev. Cancer 24, 123–140. https://doi.org/10.1038/s41568-023-00653-8

Liao, Y., Smyth, G.K., Shi, W., 2019. The R package Rsubread is easier, faster, cheaper and better for alignment and quantification of RNA sequencing reads. Nucleic Acids Res. 47, e47–e47. https://doi.org/10.1093/nar/gkz114

Lin, M.J., Svensson-Arvelund, J., Lubitz, G.S., Marabelle, A., Melero, I., Brown, B.D., Brody, J.D., 2022. Cancer vaccines: the next immunotherapy frontier. Nat. Cancer 3, 911–926. https://doi.org/10.1038/s43018-022-00418-6

Ling, P., Gately, M.K., Gubler, U., Stern, A.S., Lin, P., Hollfelder, K., Su, C., Pan, Y.C., Hakimi, J., 1995. Human IL-12 p40 homodimer binds to the IL-12 receptor but does not mediate biologic activity. J. Immunol. 154, 116–127.

Linsley, P.S., Greene, J.L., Brady, W., Bajorath, J., Ledbetter, J.A., Peach, R., 1994. Human B7-1 (CD80) and B7-2 (CD86) bind with similar avidities but distinct kinetics to CD28 and CTLA-4 receptors. Immunity 1, 793–801. https://doi.org/10.1016/S1074-7613(94)80021-9

Liu, J., Fu, M., Wang, M., Wan, D., Wei, Y., Wei, X., 2022. Cancer vaccines as promising immuno-therapeutics: platforms and current progress. J. Hematol. Oncol.J Hematol Oncol 15, 28. https://doi.org/10.1186/s13045-022-01247-x

Love, M.I., Huber, W., Anders, S., 2014. Moderated estimation of fold change and dispersion for RNA-seq data with DESeq2. Genome Biol. 15, 550. https://doi.org/10.1186/s13059-014-0550-8

Luri-Rey, C., Teijeira, Á., Wculek, S.K., De Andrea, C., Herrero, C., Lopez-Janeiro, A., Rodríguez-Ruiz, M.E., Heras, I., Aggelakopoulou, M., Berraondo, P., Sancho, D., Melero, I., 2025. Cross-priming in cancer immunology and immunotherapy. Nat. Rev. Cancer 25, 249–273. https://doi.org/10.1038/s41568-024-00785-5

Mauriello, A., Cavalluzzo, B., Ragone, C., Tagliamonte, M., Buonaguro, L., 2025. Shared neoantigens' atlas for off-the-shelf cancer vaccine development. J. Transl. Med. 23, 558. https://doi.org/10.1186/s12967-025-06478-3

Meng, M., Guo, Y., Chen, Y., Li, X., Zhang, B., Xie, Z., Liu, J., Zhao, Z., Liu, Y., Zhang, T., Qiao, Y., Shang, B., Zhou, Q., 2024. Cancer/testis-45A1 promotes cervical cancer cell tumorigenesis and drug resistance by activating oncogenic SRC and downstream signaling pathways. Cell. Oncol. 47, 657–676. https://doi.org/10.1007/s13402-023-00891-w

Merkley, S.D., Chock, C.J., Yang, X.O., Harris, J., Castillo, E.F., 2018. Modulating T Cell Responses via Autophagy: The Intrinsic Influence Controlling the Function of Both Antigen-Presenting Cells and T Cells. Front. Immunol. 9, 2914. https://doi.org/10.3389/fimmu.2018.02914

Moore, L.D., Le, T., Fan, G., 2013. DNA Methylation and Its Basic Function. Neuropsychopharmacology 38, 23–38. https://doi.org/10.1038/npp.2012.112

Morgan, M., Shepherd, L., 2025. AnnotationHub. https://doi.org/10.18129/B9.BIOC.ANNOTATIONHUB

Naik, A., Lattab, B., Qasem, H., Decock, J., 2024. Cancer testis antigens: Emerging therapeutic targets leveraging genomic instability in cancer. Mol. Ther. Oncol. 32, 200768. https://doi.org/10.1016/j.omton.2024.200768

Nesci, S., Marchi, S., Hu, J., Marincola, F.M., Algieri, C., 2025. Inflammatory mitochondrial signalling and viral mimicry in cancer. J. Transl. Med. 23, 982. https://doi.org/10.1186/s12967-025-06931-3

Palmeri, J.R., Lax, B.M., Peters, J.M., Duhamel, L., Stinson, J.A., Santollani, L., Lutz, E.A., Pinney, W., Bryson, B.D., Dane Wittrup, K., 2024. CD8+ T cell priming that is required for curative intratumorally anchored anti-4-1BB immunotherapy is constrained by Tregs. Nat. Commun. 15, 1900. https://doi.org/10.1038/s41467-024-45625-0

Patel, D., Tiusanen, V., Karttunen, K., Pihlajamaa, P., Sahu, B., 2025. Cancer cell type-specific derepression of transposable elements by inhibition of chromatin modifier enzymes. Commun. Biol. 8, 992. https://doi.org/10.1038/s42003-025-08413-0

Patsoukis, N., Wang, Q., Strauss, L., Boussiotis, V.A., 2020. Revisiting the PD-1 pathway. Sci. Adv. 6, eabd2712. https://doi.org/10.1126/sciadv.abd2712

Peche, L.Y., Ladelfa, M.F., Toledo, M.F., Mano, M., Laiseca, J.E., Schneider, C., Monte, M., 2015. Human MageB2 Protein Expression Enhances E2F Transcriptional Activity, Cell Proliferation, and Resistance to Ribotoxic Stress. J. Biol. Chem. 290, 29652–29662. https://doi.org/10.1074/jbc.M115.671982

Peng, K., Zhao, X., Fu, Y.-X., Liang, Y., 2025. Eliciting antitumor immunity via therapeutic cancer vaccines. Cell. Mol. Immunol. 22, 840–868. https://doi.org/10.1038/s41423-025-01316-4

Pujol, J.-L., Vansteenkiste, J.F., Pas, T.M.D., Atanackovic, D., Reck, M., Thomeer, M., Douillard, J.-Y., Fasola, G., Potter, V., Taylor, P., Bosquée, L., Scheubel, R., Jarnjak, S., Debois, M., De Sousa Alves, P., Louahed, J., Brichard, V.G., Lehmann, F.F., 2015. Safety and Immunogenicity of MAGE-A3 Cancer Immunotherapeutic with or without Adjuvant Chemotherapy in Patients with Resected Stage IB to III MAGE-A3-Positive Non-Small-Cell Lung Cancer. J. Thorac. Oncol. 10, 1458–1467. https://doi.org/10.1097/JTO.0000000000000653

Raza, A., Merhi, M., Inchakalody, V.P., Krishnankutty, R., Relecom, A., Uddin, S., Dermime, S., 2020. Unleashing the immune response to NY-ESO-1 cancer testis antigen as a potential target for cancer immunotherapy. J. Transl. Med. 18, 140. https://doi.org/10.1186/s12967-020-02306-y

Ren, D., Xiong, S., Ren, Y., Yang, X., Zhao, X., Jin, J., Xu, M., Liang, T., Guo, L., Weng, L., 2024. Advances in therapeutic cancer vaccines: Harnessing immune adjuvants for enhanced efficacy and future perspectives. Comput. Struct. Biotechnol. J. 23, 1833–1843. https://doi.org/10.1016/j.csbj.2024.04.054

Rowshanravan, B., Halliday, N., Sansom, D.M., 2018. CTLA-4: a moving target in immunotherapy. Blood 131, 58–67. https://doi.org/10.1182/blood-2017-06-741033

Ruiz De Morales, J.M.G., Puig, L., Daudén, E., Cañete, J.D., Pablos, J.L., Martín, A.O., Juanatey, C.G., Adán, A., Montalbán, X., Borruel, N., Ortí, G., Holgado-Martín, E., García-Vidal, C., Vizcaya-Morales, C., Martín-Vázquez, V., González-Gay, M.Á., 2020. Critical role of interleukin (IL)-17 in inflammatory and immune disorders: An updated review of the evidence focusing in controversies. Autoimmun. Rev. 19, 102429. https://doi.org/10.1016/j.autrev.2019.102429

Ruzzi, F., Riccardo, F., Conti, L., Tarone, L., Semprini, M.S., Bolli, E., Barutello, G., Quaglino, E., Lollini, P.-L., Cavallo, F., 2025. Cancer vaccines: Target antigens, vaccine platforms and preclinical models. Mol. Aspects Med. 101, 101324. https://doi.org/10.1016/j.mam.2024.101324

Salaun, B., De Saint-Vis, B., Pacheco, N., Pacheco, Y., Riesler, A., Isaac, S., Leroux, C., Clair-Moninot, V., Pin, J.-J., Griffith, J., Treilleux, I., Goddard, S., Davoust, J., Kleijmeer, M., Lebecque, S., 2004. CD208/Dendritic Cell-Lysosomal Associated Membrane Protein Is a Marker of Normal and Transformed Type II Pneumocytes. Am. J. Pathol. 164, 861–871. https://doi.org/10.1016/S0002-9440(10)63174-4

Schäfer, P., Paraschiakos, T., Windhorst, S., 2021. Oncogenic activity and cellular functionality of melanoma associated antigen A3. Biochem. Pharmacol. 192, 114700. https://doi.org/10.1016/j.bcp.2021.114700

Schmidleithner, L., Stüve, P., Feuerer, M., 2025. Transposable elements as instructors of the immune system. Nat. Rev. Immunol. 25, 696–706. https://doi.org/10.1038/s41577-025-01172-3

Schwab, R., Crow, M.K., Russo, C., Weksler, M.E., 1985. Requirements for T cell activation by OKT3 monoclonal antibody: role of modulation of T3 molecules and interleukin 1. J. Immunol. 135, 1714–1718.

Shah, B.A., Holden, J.A., Lenzo, J.C., Hadjigol, S., O'Brien-Simpson, N.M., 2025. Multi-disciplinary approaches paving the way for clinically effective peptide vaccines for cancer. Npj Vaccines 10, 68. https://doi.org/10.1038/s41541-025-01118-9

Shah, N.M., Jang, H.J., Liang, Y., Maeng, J.H., Tzeng, S.-C., Wu, A., Basri, N.L., Qu, X., Fan, C., Li, A., Katz, B., Li, D., Xing, X., Evans, B.S., Wang, T., 2023. Pan-cancer analysis identifies tumor-specific antigens derived from transposable elements. Nat. Genet. 55, 631–639. https://doi.org/10.1038/s41588-023-01349-3

Shang, R., Lee, S., Senavirathne, G., Lai, E.C., 2023. microRNAs in action: biogenesis, function and regulation. Nat. Rev. Genet. 24, 816–833. https://doi.org/10.1038/s41576-023-00611-y

Sheikhlary, S., Lopez, D.H., Moghimi, S., Sun, B., 2024. Recent Findings on Therapeutic Cancer Vaccines: An Updated Review. Biomolecules 14, 503. https://doi.org/10.3390/biom14040503

Slingluff, C.L., Petroni, G.R., Olson, W.C., Smolkin, M.E., Chianese-Bullock, K.A., Mauldin, I.S., Smith, K.T., Deacon, D.H., Varhegyi, N.E., Donnelly, S.B., Reed, C.M., Scott, K., Galeassi, N.V., Grosh, W.W., 2016. A randomized pilot trial testing the safety and immunologic effects of a MAGE-A3 protein plus AS15 immunostimulant administered into muscle or into dermal/subcutaneous sites. Cancer Immunol. Immunother. 65, 25–36. https://doi.org/10.1007/s00262-015-1770-9

Solinas, C., Gu-Trantien, C., Willard-Gallo, K., 2020. The rationale behind targeting the ICOS-ICOS ligand costimulatory pathway in cancer immunotherapy. ESMO Open 5, e000544. https://doi.org/10.1136/esmoopen-2019-000544

Soskic, B., Jeffery, L.E., Kennedy, A., Gardner, D.H., Hou, T.Z., Halliday, N., Williams, C., Janman, D., Rowshanravan, B., Hirschfield, G.M., Sansom, D.M., 2021. CD80 on Human T Cells Is Associated With FoxP3 Expression and Supports Treg Homeostasis. Front. Immunol. 11, 577655. https://doi.org/10.3389/fimmu.2020.577655

Strum, S., Andersen, M.H., Svane, I.M., Siu, L.L., Weber, J.S., 2024. State-Of-The-Art Advancements on Cancer Vaccines and Biomarkers. Am. Soc. Clin. Oncol. Educ. Book 44, e438592. https://doi.org/10.1200/EDBK_438592

Thomas, R., Al-Khadairi, G., Roelands, J., Hendrickx, W., Dermime, S., Bedognetti, D., Decock, J., 2018. NY-ESO-1 Based Immunotherapy of Cancer: Current Perspectives. Front. Immunol. 9, 947. https://doi.org/10.3389/fimmu.2018.00947

Tovar, Z., Dauphinée, M., Talal, N., 1988. Synergistic interaction between anti-CD3 and IL-2 demonstrated by proliferative response, interferon production, and non-MHC-restricted killing. Cell. Immunol. 117, 12–21. https://doi.org/10.1016/0008-8749(88)90072-X

Trinchieri, G., 2003. Interleukin-12 and the regulation of innate resistance and adaptive immunity. Nat. Rev. Immunol. 3, 133–146. https://doi.org/10.1038/nri1001

Van De Ven, K., Borst, J., 2015. Targeting the T-Cell Co-stimulatory CD27/CD70 Pathway in Cancer Immunotherapy: Rationale and Potential. Immunotherapy 7, 655–667. https://doi.org/10.2217/imt.15.32

Waldmann, T.A., 2013. The Biology of IL-15: Implications for Cancer Therapy and the Treatment of Autoimmune Disorders. J. Investig. Dermatol. Symp. Proc. 16, S28–S30. https://doi.org/10.1038/jidsymp.2013.8

Weber, J.S., Carlino, M.S., Khattak, A., Meniawy, T., Ansstas, G., Taylor, M.H., Kim, K.B., McKean, M., Long, G.V., Sullivan, R.J., Faries, M., Tran, T.T., Cowey, C.L., Pecora, A., Shaheen, M., Segar, J., Medina, T., Atkinson, V., Gibney, G.T., Luke, J.J., Thomas, S., Buchbinder, E.I., Healy, J.A., Huang, M., Morrissey, M., Feldman, I., Sehgal, V., Robert-Tissot, C., Hou, P., Zhu, L., Brown, M., Aanur, P., Meehan, R.S., Zaks, T., 2024. Individualised neoantigen therapy mRNA-4157 (V940) plus

pembrolizumab versus pembrolizumab monotherapy in resected melanoma (KEYNOTE-942): a randomised, phase 2b study. The Lancet 403, 632–644. https://doi.org/10.1016/S0140-6736(23)02268-7

Wermke, M., Araujo, D.M., Chatterjee, M., Tsimberidou, A.M., Holderried, T.A.W., Jazaeri, A.A., Reshef, R., Bokemeyer, C., Alsdorf, W., Wetzko, K., Brossart, P., Aslan, K., Backert, L., Bunk, S., Fritsche, J., Gulde, S., Hengler, S., Hilf, N., Hossain, M.B., Hukelmann, J., Kalra, M., Krishna, D., Kursunel, M.A., Maurer, D., Mayer-Mokler, A., Mendrzyk, R., Mohamed, A., Pozo, K., Satelli, A., Letizia, M., Schuster, H., Schoor, O., Wagner, C., Rammensee, H.-G., Reinhardt, C., Singh-Jasuja, H., Walter, S., Weinschenk, T., Luke, J.J., Britten, C.M., 2025. Autologous T cell therapy for PRAME+ advanced solid tumors in HLA-A*02+ patients: a phase 1 trial. Nat. Med. 31, 2365–2374. https://doi.org/10.1038/s41591-025-03650-6

Wherry, E.J., Kurachi, M., 2015. Molecular and cellular insights into T cell exhaustion. Nat. Rev. Immunol. 15, 486–499. https://doi.org/10.1038/nri3862

Wu, Z., Xue, H.-H., Bernard, J., Zeng, R., Issakov, D., Bollenbacher-Reilley, J., Belyakov, I.M., Oh, S., Berzofsky, J.A., Leonard, W.J., 2008. The IL-15 receptor α chain cytoplasmic domain is critical for normal IL-15Rα function but is not required for trans-presentation. Blood 112, 4411–4419. https://doi.org/10.1182/blood-2007-03-080697

Xie, M., Wang, J., Gong, W., Xu, H., Pan, X., Chen, Y., Ru, S., Wang, H., Chen, X., Zhao, Y., Li, J., Yin, Q., Xia, S., Zhou, X., Liu, X., Shao, Q., 2019. NF-κB-driven miR-34a impairs Treg/Th17 balance via targeting Foxp3. J. Autoimmun. 102, 96–113. https://doi.org/10.1016/j.jaut.2019.04.018

Xie, N., Shen, G., Gao, W., Huang, Z., Huang, C., Fu, L., 2023. Neoantigens: promising targets for cancer therapy. Signal Transduct. Target. Ther. 8, 9. https://doi.org/10.1038/s41392-022-01270-x

Xie, Z., Bailey, A., Kuleshov, M.V., Clarke, D.J.B., Evangelista, J.E., Jenkins, S.L., Lachmann, A., Wojciechowicz, M.L., Kropiwnicki, E., Jagodnik, K.M., Jeon, M., Ma'ayan, A., 2021. Gene Set Knowledge Discovery with Enrichr. Curr. Protoc. 1, e90. https://doi.org/10.1002/cpz1.90

Yang, W., Zhuang, J., Li, C., Cheng, G.-J., 2023. Unveiling the methyl transfer mechanisms in the epigenetic machinery DNMT3A-3 L: A comprehensive study integrating assembly dynamics with catalytic reactions. Comput. Struct. Biotechnol. J. 21, 2086–2099. https://doi.org/10.1016/j.csbj.2023.03.002

Yost, K.E., Satpathy, A.T., Wells, D.K., Qi, Y., Wang, C., Kageyama, R., McNamara, K.L., Granja, J.M., Sarin, K.Y., Brown, R.A., Gupta, R.K., Curtis, C., Bucktrout, S.L., Davis, M.M., Chang, A.L.S., Chang, H.Y., 2019. Clonal replacement of tumor-specific T cells following PD-1 blockade. Nat. Med. 25, 1251–1259. https://doi.org/10.1038/s41591-019-0522-3

Zhao, X.-R., Zong, J.-B., Liu, Y.-X., Aili, T., Qiu, M., Wu, J.-H., Hu, B., 2024. Endogenous Retroviruses Unveiled: A Comprehensive Review of Inflammatory Signaling/Senescence-Related Pathways and Therapeutic Strategies. Aging Dis. 16, 738–756. https://doi.org/10.14336/AD.2024.0123-1

Zhao, Y., Baldin, A.V., Isayev, O., Werner, J., Zamyatnin, A.A., Bazhin, A.V., 2021. Cancer Vaccines: Antigen Selection Strategy. Vaccines 9, 85. https://doi.org/10.3390/vaccines9020085

Zhao, Y., Harrison, D.L., Song, Y., Ji, J., Huang, J., Hui, E., 2018. Antigen-Presenting Cell-Intrinsic PD-1 Neutralizes PD-L1 in cis to Attenuate PD-1 Signaling in T Cells. Cell Rep. 24, 379-390.e6. https://doi.org/10.1016/j.celrep.2018.06.054